DIRECTION OF ARRIVAL ESTIMATION BY ARRAY INTERPOLATION IN RANDOMLY DISTRIBUTED SENSOR ARRAYS

A THESIS SUBMITTED TO
THE GRADUATE SCHOOL OF NATURAL AND APPLIED SCIENCES
OF
THE MIDDLE EAST TECHNICAL UNIVERSITY

BY

IŞIN AKYILDIZ

IN PARTIAL FULFILLMENT OF THE REQUIREMENTS
FOR
THE DEGREE OF MASTER OF SCIENCE
IN
ELECTRICAL AND ELECTRONICS ENGINEERING

DECEMBER 2006

Approval of the Graduate School of Natural and Applied Sciences

Prof. Dr. Canan ÖZGEN
Director

I certify that this thesis satisfies all the requirements as a thesis for the degree of Master of Science.

Prof. Dr. İsmet ERKMEN
Head of Department

This is to certify that we have read this thesis and that in our opinion it is fully adequate, in scope and quality, as a thesis for the degree of Master of Science.

Assoc. Prof. Dr. Engin TUNCER
Supervisor

Examining Committee Members

Prof. Dr. Kemal LEBLEBİCİOGLU	(METU, EEE)	_____
Assoc. Prof. Dr. Engin TUNCER	(METU, EEE)	_____
Assoc. Prof. Dr. Gözde BOZDAĞI	(METU, EEE)	_____
Asst. Prof. Dr. Afşar SARANLI	(METU, EEE)	_____
M. Sc. Aykut ARIKAN	(ASELSAN)	_____

I hearby declare that all information in this document has been obtained and presented in accordance with academic rules and ethical conduct. I also declare that, as required, I have fully cited and referenced all material and results that are not original to this work.

Name Lastname : Işın AKYILDIZ

Signature :

ABSTRACT

DIRECTION OF ARRIVAL ESTIMATION BY ARRAY INTERPOLATION IN RANDOMLY DISTRIBUTED SENSOR ARRAYS

AKYILDIZ, Işın
M.Sc., Department of Electrical and Electronics Engineering
Supervisor: Assoc. Prof. Dr. Engin TUNCER

December 2006, 78 pages

In this thesis, DOA estimation using array interpolation in randomly distributed sensor arrays is considered. Array interpolation is a technique in which a virtual array is obtained from the real array and the outputs of the virtual array, computed from the real array using a linear transformation, is used for direction of arrival estimation. The idea of array interpolation technique is to make simplified and computationally less demanding high resolution direction finding methods applicable to the general class of non-structured arrays. In this study, two different interpolation technique is applied for arbitrary array geometries in an attempt to extend root-MUSIC algorithm to arbitrary array geometries. Another issue of array interpolation related to direction finding is spatial smoothing in the presence of multipath sources. It is shown that due to the Vandermonde structure of virtual array manifold vector obtained from the proposed interpolation methods, it is pos-

sible to use spatial smoothing algorithms for the case of multipath sources.

Keywords: Direction of Arrival Estimation, Root-MUSIC, Randomly Distributed, Array Interpolation, Spatial Smoothing

ÖZ

DÜZENSİZ DİZİLERDE DİZİ ARADEĞERLENDİRME İLE GELİŞ AÇISI TAHMİNİ

AKYILDIZ, Işın
Yüksek Lisans, Elektrik ve Elektronik Mühendisliği Bölümü
Tez Yöneticisi: Doç. Dr. Engin TUNCER

Aralık 2006, 78 sayfa

Düzensiz dizilerde dizi aradeğerlendirme ile geliş açısı tahmini ele alınmıştır. Dizi aradeğerlendirme tekniğinde, gerçek dizi kullanılarak sanal dizi elde edilir ve sanal dizinin alıcı çıktıları geliş açısı tahmini için kullanılır. Dizi aradeğerlendirmenin ana amacı basitleştirilmiş ve işlemsel olarak daha az kompleks olan yüksek çözünürlüklü geliş açısı tahmin metodlarını genel düzenli yapısı olmayan dizilere de uygulanabilir hale getirmektir. Bu çalışmada düzensiz yerleştirilmiş bir alıcı dizini üzerinde aradeğerlendirme yapılmış ve kök MUSIC algoritması kullanılarak geliş açısı tahmin performansı değerlendirilmiştir. Açı aradeğerlendirme tekniğinin diğer bir avantajıda çok yönlü enerji kaynakları durumunda uzaysal yumuşatma algoritmalarının kullanılabilirliğidir. Sanal dizi çıktı (manifold) vektörünün özel Vandermonde yapısı sebebiyle uzaysal yumuşatma metodlarının kullanılabilirliği üzerinde durulmuştur.

Anahtar sözcükler: Geliş Açısı Tahmini, Düzensiz Diziler, Dizi Aradeğer-

lendirmesi, Kök MUSIC, uzaysal yumuşatma

to my family and Alper

ACKNOWLEDGMENTS

I would like to express my sincere gratitude to my supervisor Doç. Dr. Temel Engin Tuncer for his supervision, guidance and encouragement throughout this study.

Special thanks to my beloved Alper for his help during the preparation of the thesis and his great encouragement during this period. Also special thanks to my friend Kaya for his great support and assistance during the preperation of the thesis. I would like to deeply thank to my friend Zeynep, for her drawings in the thesis.

I am forever indepted to my family who have been supporting me in every aspect of my life.

I would like to express my appreciation to my colleagues for their valuable support.

TABLE OF CONTENTS

LIST OF FIGURES

CHAPTER 1

INTRODUCTION

Array signal processing deals with the processing of information bearing signals collected by an array of sensors operating in a physical environment of interest in order to execute an estimation task. Identifying the location of targets or the direction of arrival (DOA) of any signal is one of the defined estimation tasks. In the DOA estimation problem, the data from the target, i.e., the source of energy, which may be electromagnetic wave, acoustic wave or seismic wave, etc, is processed in order to obtain its location or DOA angle. The sensor array can be passive or active. In a passive system, the sensor array has the task of listening to the environment. In this case, the energy source is the target itself. In an active system, on the other hand, a transmitter emits energy to the environment and the sensor array listens to the environment for the response of the target. The sensors may have several forms depending on the type of energy radiated from the target. They may be antennas as in RADAR, radio communications and radio astronomy, or hydrophones as in SONAR, or geophones as in seismology, or microphones as in acoustics, or x-ray detectors as in medical imaging. Independent of their type, the sensors are designed to provide an interface between the physical environment in which the array is embedded and signal processing part of the system. The role of the sensors in an array signal processing system is to convert the physical energy to the electrical signals and the function of the processor is to produce the estimates of the target parameters of interest by using the information contained in the electrical signals. The target param-

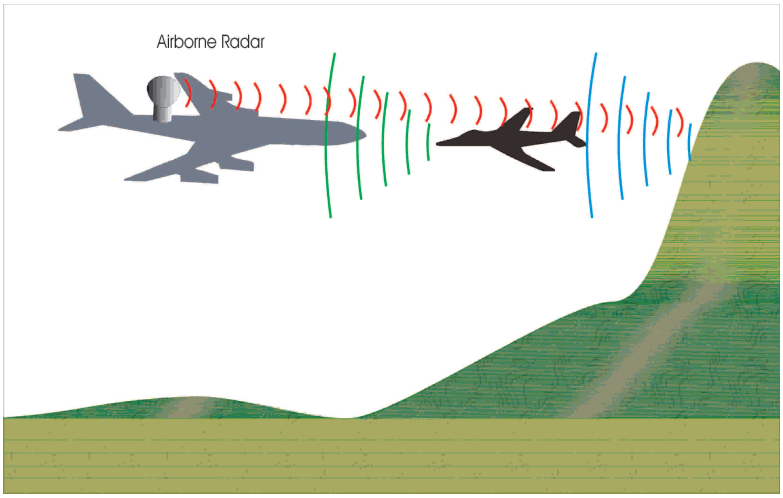

Figure 1.1: Airborne RADAR

eters of interest may be the shape of the target, the DOA of the target or the number of sources.

Array signal processing is very important in RADAR, SONAR, seismic systems, electronic surveillance, medical diagnosis and treatment and radio astronomy.

In RADAR, antenna array is used for both transmission and reception of signals. Some military applications of antenna array systems include phased array RADAR systems which are used for ballistic missile detection.

Antenna arrays are widely used in radio astronomy area. A radio astronomy array system is a passive array system which is used for the detection of celestial objects and the estimation of their characteristics.

Arrays are widely used in SONAR systems. There are two types of SONAR system which are active and passive SONAR. In active SONAR, acoustic energy is transmitted in water and the reflections from the target listened by the array system are processed in order to detect the target. The theory of active SONAR has very much in common with active RADAR.

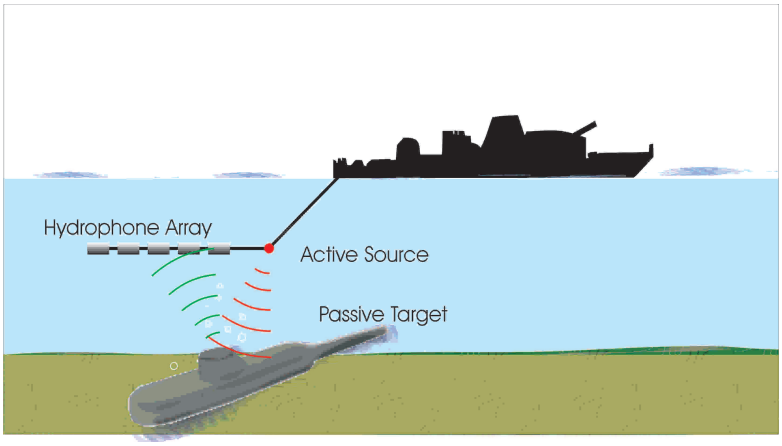

Figure 1.2: Rescue SONAR

Passive SONAR systems only listen to the water for the acoustic energy caused by the active target and process the data obtained from the target in order to locate the target. A good example for hydrophone array system application is the towed array which is towed from the hull of a ship in order to listen to the ocean to detect torpedoes. In Figure 1.3 such a towed array system is shown.

There are two areas of seismology in which array signal processing plays an important role. First one is the detection and the localization of the underground explosions. The second area is the exploration seismology. In the exploration seismology, an active source transmits energy to the subsurface and the seismic array on the surface listens to the echoes and constructs the image of the subsurface in which the structure and physical properties are described.

Independent from the type of energy transmitted from the target, the direction finding (DF) or DOA estimation problem is theoretically defined as the estimation of the propagation direction of a wave. Due to its widespread application and difficulty of obtaining optimum estimator, the topic has re-

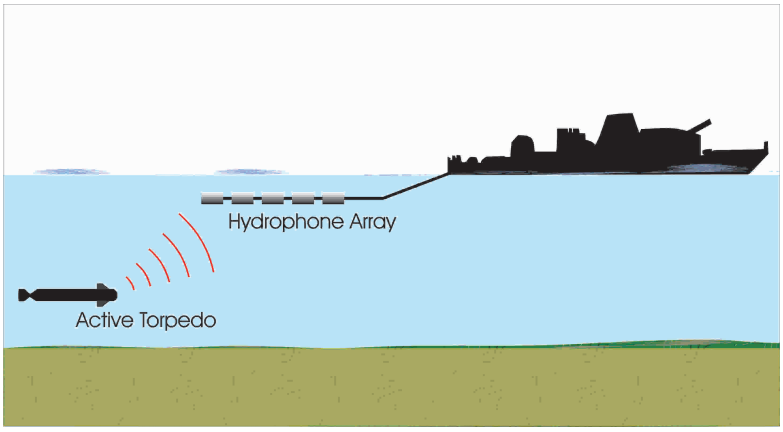

Figure 1.3: Towed Array

ceived a significant amount of attention over the last several decades and a large quantity of algorithms for different scenarios for a variety of array structures have been developed.

The DOA estimation techniques can be classified into two main categories, namely the spectral-based and the parametric approach. In the spectral based approach, a spectrum-like function for DOAs are formed and the values at which the function in question gives peaks are found as the DOA estimates. In the parametric approach, the signal waveforms are modeled as random processes and the DOA estimates are found by minimizing some statistical functions parameterized by the DOAs. The parametric approach results in more accurate estimates. However, the parametric techniques are computationally much more demanding compared to spectral-based techniques. The usage of the parametric techniques is preferable for the case when coherent sources are involved in the DOA estimation problem. The spectral-based techniques can also be grouped under two different subclasses, the beamforming techniques and the subspace-based techniques.

In beamforming techniques, the main idea is to steer the array and measure the output power. The points at which the output power give peaks are

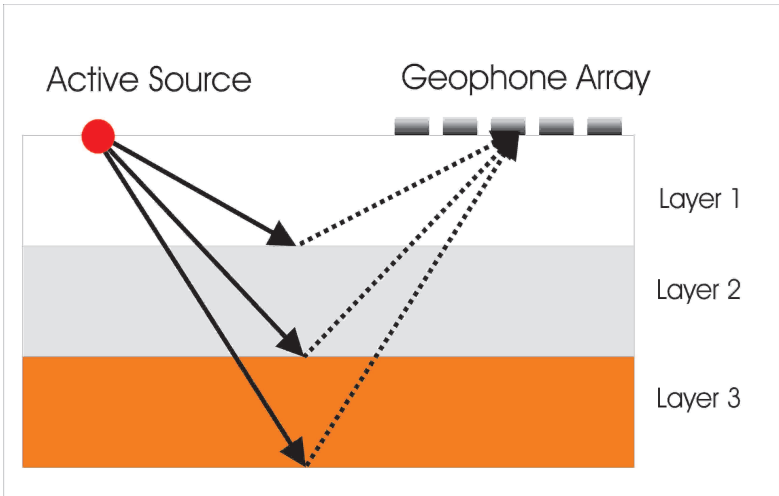

Figure 1.4: Geophone Array

recorded as the DOA estimates. The conventional beamformer, namely the Bartlett beamformer is introduced by Bartlett in [2] and is a general extension of the fourier-based spectral analysis. It is further developed by Capon in [7], in order to improve resolution capability of the beamformer for two closely spaced sources.

In subspace-based techniques, the eigen-structure of the observed data covariance matrix is directly used in order to find the DOA estimates. The first subspace-based algorithm is called MUSIC (Multiple Signal Classification), and was introduced by Schmidt in [24], [25], [26] and independently by Bienvenu and Kopp in [3] and [4]. For standard linear arrays, root-MUSIC and ESPRIT (Estimation of Signal Parameters via Rotational Invariance) is introduced in [1], [19] and [22], respectively. The subspace-based algorithms have an increased resolution compared to beamforming techniques, due to the fact that no windowing of the data is required.

The spectral-based methods are computationally less demanding than the parametric methods. However, especially for the scenarios involving highly

correlated signals, the performance of spectral-based methods may be insufficient. The parametric methods yield more accurate solutions. Unfortunately, these methods require multidimensional search to find the estimates, which is computationally quite complex. The most well known and frequently used parametric algorithm is the Maximum Likelihood (ML) technique [28].

Another important classification of the DOA estimation approaches can be done depending on the array geometry which is required for the technique used. The array with special arrangement of sensors, especially the uniform linear array (ULA) gives the opportunity to use high resolution, computationally less demanding and simplified subspace-based techniques like root-MUSIC, RARE, IQML, conventional and multiple invariance ESPRIT. All this algorithms require uniform linear arrays and/or array geometries with shift-invariances.

Another central problem in the area of the array processing related to the DOA is the DOA estimation in the case of fully correlated plane waves or signals. This case referred as the coherent signal case, appears in specular multipath propagation and has been therefore gained great practical importance. A preprocessing technique called spatial smoothing for dealing with coherent signals which allows the use of low-complexity DOA methods for only ULA is proposed by Evans et al. and Shan et al. in [8] and in [27] further developed by Pillai in [20].

None of the mentioned algorithms can be utilized for the case of array geometries different than ULA. In an attempt to exploit these computationally less demanding and simplified high resolution algorithms for the general class of array geometries, the concept of array interpolation is introduced to the literature by Friedlander in [10] and [12]. The array interpolation is a technique in which a virtual array is obtained from the real array and the outputs of the virtual array, computed from the real array using a linear transformation, is used for direction of arrival estimation. The interpolated

array concept not only broadened the mentioned algorithms to the general class of array geometries but also have many other advantages, like the expansion of spatial smoothing preprocessing technique to the randomly distributed array geometries. The interpolated spatial smoothing technique is introduced to the literature by Friedlander in [11].

In this work, the DOA estimation problem in randomly distributed sensor arrays by using two different interpolation methods is considered. The first method is the array interpolation method with virtual ULA and introduced by Friedlander in [10]. In the second array interpolation method a virtual array manifold vector is used for the DOA estimation [6]. As mentioned in the subsequent paragraph, the aim of the array interpolation is the separation to some extent the DOA estimation problem from the physical locations of the array elements. This is done by obtaining a virtual array from the real array by a linear interpolation technique and the DOA estimation is done by using outputs from the virtual array elements rather than the real array elements. The two interpolation methods considered in this work differ in the selection of virtual array. In the first method, the virtual array is a uniformly spaced array, the design of which is under the control of the designer with some restrictions. However, the virtual array is not a physical array in the second method. It is obtained from the real array manifold vector by using arc length approximation. The steps involved in the virtual array creation and interpolation matrix design are considered in detail for the two interpolation methods. The root-MUSIC algorithm is used for the DOA estimation. The spatial preprocessing technique is used for the DOA estimation when the sources are correlated. The interpolated spatial smoothing techniques are introduced to the literature by Friedlander for virtual ULA in [11]. However, in this application, the spatial smoothing preprocessing technique is applied to a non-physical virtual array having the necessary Vandermonde structure.

The work is organized as follows. In Chapter 2, some preliminary knowl-

edge on wave equation is given. The array response to an external signal field is mathematically formulated in order to obtain the stochastic model used for the DOA estimation with the narrowband assumption on sources. The array manifold vector concept is introduced. In Chapter 3, the array manifold vector for ULA is obtained. The Vandermonde structure of array manifold vector for ULA is emphasized and the formulization of the root-MUSIC algorithm and the spatial smoothing algorithm for the correlated sources case are given. In Chapter 4, virtual array concept is introduced. The two interpolation methods for the interpolation matrix design are explained in detail. The interpolated root-MUSIC and the interpolated spatial smoothing algorithms are mathematically formulized. In Chapter 5, the simulation results for the performance analysis of the interpolated root-MUSIC with the two interpolation methods and the spatial smoothing preprocessing are presented. Finally, in Chapter 6, the conclusion is provided.

CHAPTER 2

PRELIMINARIES

As stated in the previous chapter, in the DOA estimation problem the data from the target may be electromagnetic wave, sound wave, or seismic wave, etc. However, in this thesis the DOA estimation problem for acoustic sources is investigated. In this chapter, the sound wave equation and its solution for plane waves with narrowband assumption is given and the response of a microphone array system to this source is formulized. The array output data model for the DOA estimation with narrowband assumption on sources is obtained.

2.1 Source

General equation of a sound wave in three dimensional space is given as

$$\Delta^2 p(\xi, t) = \frac{1}{c^2} \frac{\partial^2 p(\xi, t)}{\partial t^2} \tag{2.1}$$

where c is the speed of sound, ξ is the three-dimensional space coordinates and t is time variable. In the discussion, it is assumed that the sound sources are in the far-field, i.e., they are far enough so that the solution of wave equation gives plane waves. For this case, the solution of the wave equation for planar real sound wave is mathematically expressed as

$$p(\xi) = P_1 e^{j(\omega/c)\xi} + P_2 e^{-j(\omega/c)\xi} \tag{2.2}$$

It is also assumed that the media where the sound waves propagate is homogeneous, i.e., the speed of plane waves is independent from the coordinates

of the propagation region. The incoming signal is just a complex exponential at the fixed frequency ω.

2.2 Sensor Array

Microphone sensor arrays have arbitrary geometry and they are positioned in xy-plane as shown in Figure 2.1. The sensor positions should satisfy the sampling theorem. This means that the array elements must be less than a half wavelength apart. The plane wave and the sensor array are assumed to be on the same plane. Another assumption is that all microphones are calibrated with the known frequency response and they are isotropic, i.e., their response is independent of the DOA of the sources.

2.3 Array Response

The array output model is the central part of DOA estimation problem. The array response of a microphone array to a plane wave is formulized in this section. The array consists of isotropic sensors with the known frequency response. The sensors in Figure 2.1 spatially sample the signal field at the locations p_n:n= 0, 1, $\ldots$, $m-1$. This yields a set of signals denoted by $\overrightarrow{f}(t, \overrightarrow{p})$

$$\overrightarrow{f}(t, \overrightarrow{p}) = \begin{pmatrix} f(t, p_0) \\ f(t, p_1) \\ \vdots \\ f(t, p_{m-1}) \end{pmatrix} \tag{2.3}$$

Assuming that the impulse response of the n^{th} sensor is $h_n(t)$ and n^{th} sensor output is $y_n(t)$, the sensor impulse response vector and the sensor output

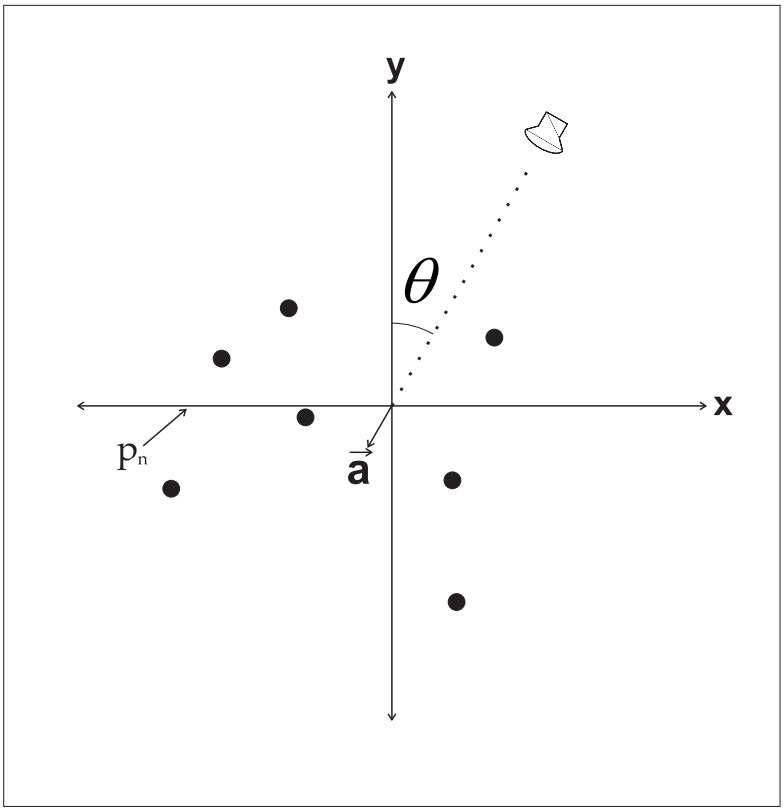

Figure 2.1: m-element randomly distributed array

vector is given as

$$\overrightarrow{h}(T) = \begin{pmatrix} h_0(T) \\ h_1(T) \\ \vdots \\ h_{m-1}(T)) \end{pmatrix} \text{ and } \overrightarrow{y}(t) = \begin{pmatrix} y_0(t) \\ y_1(t) \\ \vdots \\ y_{m-1}(t)) \end{pmatrix} \tag{2.4}$$

$$y_n(t) = h_n(t) * f(t - T_n) = \int_{-\infty}^{+\infty} h_n(t - T) f(T, p_n) dT \tag{2.5}$$

Taking the Fourier Transform of both sides and expressing the equation in the Fourier domain yields

$$Y_n(w) = H_n(w) F(w, p_n) \tag{2.6}$$

where the input is assumed to be a plane wave propagating in the direction a with center (frequency f) radian frequency w and c is the speed of the propagation in the air (or in the medium). If $f(t)$ is the signal received at the origin of the coordinate system (or the center of gravity of sensors), then the signals impinging on the sensors are the delayed versions of $f(t)$. The vector of arriving signals can be written as

$$\overrightarrow{f}(t, \overrightarrow{p}) = \begin{pmatrix} f(t - T_0) \\ f(t - T_1) \\ \vdots \\ f(t - T_{m-1}) \end{pmatrix} \text{ where } T_n = \frac{a^T p_n}{c} \text{ and } a = \begin{pmatrix} -cos(\theta) \\ -sin(\theta) \end{pmatrix} \tag{2.7}$$

where T_n is the time delay corresponding to the time of arrival at the n^{th} sensor and T_n is given as

$$T_n = \frac{-x_n cos(\theta) - y_n sin(\theta)}{c} \text{ where } p_n = \begin{pmatrix} x_n \\ y_n \end{pmatrix} \tag{2.8}$$

Expressing sensor output equation (2.5) in Fourier Domain yields

$$Y_n(w) = H_n(w)F(w, p_n) = H_n(w)e^{-jwT_n}F(w) = H_n(w)e^{j\frac{w(x_n cos(\theta)+y_n sin(\theta))}{c}}F(w) \tag{2.9}$$

For a plane wave propagating in the direction a with the radian frequency w with propagation speed c the wavenumber vector is defined as

$$\overrightarrow{k} = \overrightarrow{a}\frac{2\pi}{\lambda} \text{ and } k = \| \overrightarrow{k} \| = \frac{2\pi}{\lambda} \tag{2.10}$$

Then the above equation can be written as

$$Y_n(w) = H_n(w)e^{j\frac{2\pi(x_n cos(\theta)+y_n sin(\theta))}{\lambda}}F(w) \tag{2.11}$$

If the sensor coordinates are given in terms of wavelength, then (2.11) can be rewritten as

$$Y_n(w) = H_n(w)e^{j2\pi(x_n cos(\theta)+y_n sin(\theta))}F(w) \tag{2.12}$$

Assuming that all the sensors are identical and their frequency response at w is the same and $H(w)$, then the sensor output vector can be expressed as

$$\overrightarrow{Y}(w) = H(w)F(w)\begin{pmatrix} e^{j2\pi(x_0 cos(\theta)+y_0 sin(\theta))} \\ e^{j2\pi(x_1 cos(\theta)+y_1 sin(\theta))} \\ e^{j2\pi(x_2 cos(\theta)+y_2 sin(\theta))} \\ \vdots \\ e^{j2\pi(x_{m-1} cos(\theta)+y_{m-1} sin(\theta))} \end{pmatrix} \tag{2.13}$$

The matrix in (2.14) is called as the Array Manifold Vector

$$a(\theta) = \begin{pmatrix} e^{j2\pi(x_0 cos(\theta)+y_0 sin(\theta))} \\ e^{j2\pi(x_1 cos(\theta)+y_1 sin(\theta))} \\ e^{j2\pi(x_2 cos(\theta)+y_2 sin(\theta))} \\ \vdots \\ e^{j2\pi(x_{m-1} cos(\theta)+y_{m-1} sin(\theta))} \end{pmatrix} \tag{2.14}$$

Since it is assumed that $f(t)$ is a plane wave propagating in the direction a with radian frequency w with the propagation speed c, the equation in (2.13) also holds in time domain, i.e.,

$$\overrightarrow{y}(t) = H(w)f(t) \begin{pmatrix} e^{j2\pi(x_0 cos(\theta)+y_0 sin(\theta))} \\ e^{j2\pi(x_1 cos(\theta)+y_1 sin(\theta))} \\ e^{j2\pi(x_2 cos(\theta)+y_2 sin(\theta))} \\ \vdots \\ e^{j2\pi(x_{m-1} cos(\theta)+y_{m-1} sin(\theta))} \end{pmatrix} \tag{2.15}$$

In the classical array theory the output for a plane wave propogating in the direction a with radian frequency w with the propagation speed c, the output at each sensor is given by (2.15) .

For obtaining the output sensor equation in time domain, the main assumption is that our plane waves are propagating at single frequency. In the next subsection, it is shown that when the waves are narrowband, then the same equation still holds. The assumption is called as the narrowband assumption.

2.3.1 The Narrowband Assumption

The sensor output equation is obtained for the case when the plane waves are bandpass signals. In this case, the signal at a location p_n is expressed as

$$f(t, p_n) = \sqrt{2} Re\{f(t, p_n) e^{j w_c t}\} \text{ where } n = 0, 1, \ldots, m-1 \tag{2.16}$$

where w_c is the carrier frequency and $f(t, p_n)$ is the complex envelope. Assuming that the complex envelope is band-limited to the region

$$w_l \leq 2\pi B/2 \tag{2.17}$$

$$f(t,p_n) = \sqrt{2}Re\{f(t,p_n)e^{jw_c t}\} \;\; n = 0,1,\ldots,m-1 \tag{2.18}$$

and πB is the maximum bandwidth of the complex envelope. For the plane wave in (2.16), (2.18) becomes

$$f(t,p_n) = \sqrt{2}Re\{f(t-T_n)e^{jw_c(t-T_n)}\} \text{ where } n = 0,1,\ldots,m-1 \tag{2.19}$$

where T_n is given by (2.7). Considering the travel time of the wave across the array, maximum travel time across the array is the travel time between the two furthest away element of the array. If δT_{max} is the maximum travel time delay, then all $T_n \leq \delta T_{max}$. If the bandwidth of the complex envelope is small enough

$$f(t-T_n) \approx f(t) \text{ requiring that } B\delta T_{max} \leq 1 \tag{2.20}$$

This is called the narrowband assumption. For this case, the sensor outputs are expressed as in the deterministic case and array manifold vector is used for the sensor output data model.

$$\overrightarrow{y}(t) = H(w_c)f(t) \begin{pmatrix} e^{j2\pi(x_0 cos(\theta)+y_0 sin(\theta))} \\ e^{j2\pi(x_1 cos(\theta)+y_1 sin(\theta))} \\ e^{j2\pi(x_2 cos(\theta)+y_2 sin(\theta))} \\ \vdots \\ e^{j2\pi(x_{m-1} cos(\theta)+y_{m-1} sin(\theta))} \end{pmatrix} \tag{2.21}$$

2.3.2 The Array Output Model

After obtaining sensor output equation for the deterministic case, the array output model with the narrowband assumption is constructed in order to use for the DOA estimation. The equations are converted to the discrete time domain. In the previous section, it is assumed that there is no sensor noise on the sensor outputs. In this section, measurement noise is added to the system model. It is assumed that the measurement noise has a common

variance ${\sigma_n}^2$ at all sensors and uncorrelated among all the sensors. Such noise is termed as spatially white and it is a reasonable model for a receiver noise.

Let an array of m sensors receive n narrowband plane waves from far-field emitters with the same center frequency f_c. The signal model is

$$x(t) = A(\theta)s(t) + n(t) \tag{2.22}$$

where

$$A(\theta) = \Big(\; a(\theta_1) + \alpha a(\theta_2) \quad a(\theta_3) \quad \ldots \quad a(\theta_n) \; \Big)^T \tag{2.23}$$

$s(t)$ is a vector containing the complex signal envelopes of n narrowband signal sources located in the xy plane, $n(t)$ is mX1 vector of zero mean spatially white sensor noise of variance ${\sigma_n}^2$ and the columns of the array manifold matrix or the array steering matrix $A(\theta)$ are the array manifold vectors or array steering vectors $a(\theta_l)$ corresponding to the unknown source DOAs $\theta_1,\ \theta_2,\ .,\ .,\ \theta_n$

The covariance matrix corresponding to (2.22) is given as

$$R = E\{x(t)x(t)^H\} = A(\theta)SA^H(\theta) + {\sigma_n}^2 I \tag{2.24}$$

where S is the source covariance matrix.

2.3.3 The Array Output Model: Coherent Sources Case

A crucial problem in the area of the DOA is the estimation of the direction of arrival in the case of fully correlated signals. This case, referred as the coherent signal case and appears in specular multipath propagation. Therefore it has a great practical importance. In this section, the effect of the coherence of the sources on the array output model is explained, before proceeding to explain the solution for this paramount problem in the successive chapters.

The array output model is given by (2.22). In this equation, $s(t)$ is a vector containing the complex signal envelopes of n narrowband signal sources located in the xy plane, $n(t)$ is mX1 vector of zero mean spatially white sensor noise of variance ${\sigma_n}^2$ and the columns of the array manifold matrix or the array steering matrix $A(\theta)$ are the array manifold vectors or array steering vectors $a(\theta_l)$ corresponding to the unknown source DOAs.

$$A(\theta) = \begin{pmatrix} a(\theta_1) & a(\theta_2) & \dots & a(\theta_n) \end{pmatrix} \tag{2.25}$$

$$s(t) = \begin{pmatrix} s_1(t) & s_2(t) & \dots & s_n(t) \end{pmatrix}^T \tag{2.26}$$

For simplicity,it is assumed that only two sources are coherent, i.e., $s_1(t)$ and $s_2(t)$, so that $s_2(t)$ is a scaled and delayed version of $s_1(t)$. The coherence of sources can be mathematically expressed as

$$s_2(t) = \alpha s_1(t) \tag{2.27}$$

where $\alpha = \beta e^{(j\phi)}$

Substituting (2.26) to (2.27),

$$s(t) = \begin{pmatrix} (1+\alpha)s_1(t) & s_3(t) & \dots & s_n(t) \end{pmatrix}^T \tag{2.28}$$

is obtained. $s(t)$ is reduced to $(n-1)$X1 matrix and $A(\theta)$ is also reduced to $(n-1)$Xm matrix, i.e.,

$$A(\theta) = \begin{pmatrix} a(\theta_1) + \alpha a(\theta_2) & a(\theta_3) & \dots & a(\theta_n) \end{pmatrix}^T \tag{2.29}$$

$S = E\{s(t){s(t)}^H\}$, the covariance matrix of the modified signals, is a $(n-1)$X$(n-1)$ nonsingular matrix and $A(\theta)$ is a matrix with full column rank. On the contrary, in the non-modified form it is singular with rank $n-1$. Due to this singularity the high resolution eigen-structure based DOA estimation algorithms can't be used with the signal covariance matrix. The spatial smoothing preprocessing to solve this problem is mentioned in section 2.3 for ULA and is discussed for the general non-structured arrays by array interpolation in the successive chapters.

CHAPTER 3

A SPECIAL ARRAY GEOMETRY: ULA

Uniform Linear Arrays take a very large part of the DOA estimation problem. Considering any problem encountered in DOA estimation, the starting point of the researchers is always well structured array geometries, especially ULA. Looking at the literature; many computationally less demanding and simplified high resolution techniques were developed like root-MUSIC, RARE etc. for the ULA. The most critical problem, signal coherence, is also solved for the ULA case in an attempt to use eigen-structure based DOA estimation algorithms. Looking at all of the work done on ULA, the question of what makes ULA so special readily arises in a researcher's mind. None of the mentioned algorithms can be exploited for the case of array geometries different than ULA.

In an attempt to exploit these computationally less demanding and simplified high resolution algorithms for the general class of array geometries, the concept of array interpolation is introduced to the literature by Friedlander in [10]. Array interpolation is a technique in which a virtual array is obtained from the real array and the outputs of the virtual array, computed from the real array using a linear transformation, are used for DOA estimation. The interpolated array concept not only extended the eigen-structure based algorithms to the general class of array geometries but also have many other advantages, like the expansion of spatial smoothing preprocessing technique

to the randomly distributed array geometries.

In this chapter, array output data model for ULA is obtained and the mathematical formulization of root-MUSIC and spatial smoothing algorithm is given in order to emphasize the properties of ULA which make it possible to use these algorithms.

3.1 Array Manifold Vector:ULA Case

In chapter 2, the array output model for a m element sensor array is obtained and is given by (2.22).

In the model, the only term affected by sensor positions is array manifold vector, i.e., if there is a difference for the ULA case, this is the array manifold vector structure which makes this difference.

The linear array of interest is shown in Figure 3.1. There are m elements located on the x-axis with uniform spacing equal to d in terms of wavelength of the plane wave impinging on the sensor array. The origin of the coordinate is taken as the center of gravity of the sensor positions. The choice of centering only leads to a phase difference on the array manifold vector.

$$p_n = \begin{pmatrix} x_n \\ y_n \end{pmatrix} \text{ where } x_n = (n - \frac{m-1}{2}) \text{ and } y_n = 0 \text{ sensors on the x axis} \tag{3.1}$$

Substituting the position vector (2.22) to the array manifold equation (2.14)

$$a(\theta) = \begin{pmatrix} e^{j2\pi(-\frac{(m-1)}{2})dcos(\theta)} \\ e^{j2\pi(1-\frac{(m-1)}{2})dcos(\theta)} \\ e^{j2\pi(2-\frac{(m-1)}{2})dcos(\theta)} \\ \vdots \\ e^{j2\pi(\frac{(m-1)}{2})dcos(\theta)} \end{pmatrix} \tag{3.2}$$

Taking $e^{-j2\pi(\frac{(m-1)}{2})dcos(\theta)}$ pharantesis

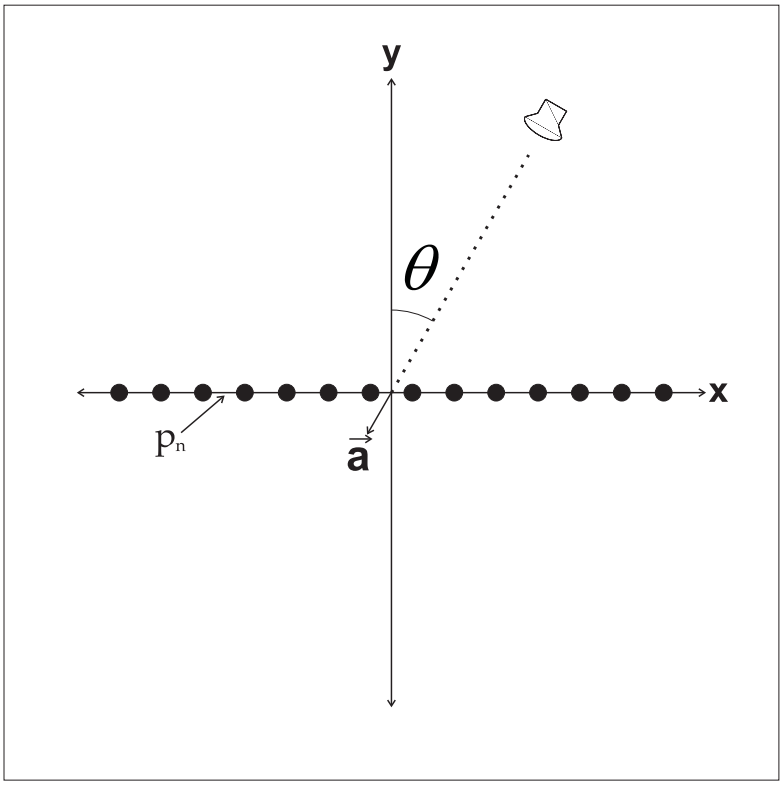

Figure 3.1: m-element uniform linear array

$$a(\theta) = e^{-j2\pi(\frac{(m-1)}{2})dcos(\theta)} \begin{pmatrix} 1 \\ e^{j2\pi dcos(\theta)} \\ e^{j2\pi 2dcos(\theta)} \\ \vdots \\ e^{j2\pi(m-1)dcos(\theta)} \end{pmatrix} \tag{3.3}$$

by substituting

$$\psi = g(\theta) = 2\pi dcos(\theta) \text{ then } a(\theta) = e^{-j(\frac{(m-1)}{2})\psi} \begin{pmatrix} 1 \\ e^{j\phi} \\ e^{j2\phi} \\ \vdots \\ e^{j(m-1)\phi} \end{pmatrix} \tag{3.4}$$

This form emphasizes The Vandermonde structure.

$$A(\theta) = \begin{pmatrix} a(\theta_1) & a(\theta_2) & \dots & a(\theta_{n-1}) \end{pmatrix} \tag{3.5}$$

and it is known

$$R = E\{x(t)x(t)^H\} = A(\theta)SA^H(\theta) + {\sigma_n}^2 I \tag{3.6}$$

S, signal covariance matrix is *diagonal*(implies *nonsingularity*) when the signals $s(t) = \begin{pmatrix} s_1(t) & s_2(t) & \dots & s_n(t) \end{pmatrix}^T$ are uncorrelated, *nondiagonal* and *nonsingular* when the signals are *partiallycorrelated*, and *nondiagonal* and *singular* when some signals are fully correlated.

Assuming that the spacing d between the sensors is less than half a wavelength it follows that the columns of the matrix A are all different and due to the Vandermonde structure, linearly independent. Thus, if S is *nonsingular*, then the rank of R is n. If

$$\lambda_1 \geq \lambda_2 \geq \lambda_3 .... \geq \lambda_n \tag{3.7}$$

with corresponding eigenvectors

$$v_1,\ v_1,\ v_2 \ldots,\ v_n \tag{3.8}$$

All of this rank properties imply two important properties, which are the basics of subspace based algorithms.

1-) the minimal eigenvalue of R is equal to σ^2 with multiplicity $(m-n)$

$$\lambda_{n+1} = \lambda_{n+2} = \lambda_{n+3} .... = \lambda_m = \sigma^2 \tag{3.9}$$

2-) the eigenvectors corresponding to the minimal eigenvalue are orthogonal to the columns of the A matrix, i.e. the direction vectors of the signals.

$$\{v_{n+1},\ v_{n+2},\ v_{n+3} \ldots,\ v_m\} \perp \{a(\theta_1), a(\theta_2), a(\theta_2) \ldots,\ a(\theta_m)\} \tag{3.10}$$

the subspace spanned by the eigenvectors corresponding to the smallest eigenvalue is referred as the "noise" subspace and its orthogonal complement, spanned by the direction vectors is referred as the signal subspace. The high resolution eigenstructure techniques are based on the exploitation of properties (3.9) and (3.10)

3.2 The root-MUSIC Algorithm

In this section, the formulization of the root-MUSIC is shortly given for ULA.

For a standard linear array manifold, a standart polynomial representation can be used. Array manifold vector is written as

$$\psi = g(\theta) = 2\pi d cos(\theta) \text{ then } a(\theta) = e^{-j(\frac{(m-1)}{2})\psi} \begin{pmatrix} 1 & e^{j\psi} & e^{j2\psi} & \ldots & e^{j(m-1)\psi} \end{pmatrix}^T \tag{3.11}$$

by putting in the array manifold vector $z = e^{j\psi}$

$$a(z) = z^{-\frac{m-1}{2}} \begin{pmatrix} 1 & z & z^2 & \ldots & z^{m-1} \end{pmatrix}^T \tag{3.12}$$

Signal subspace and noise subspace are respectively defined as U_S and U_N

$$U_S \triangleq [\ v_1 \mid v_2 \mid \ \ldots\ v_n\ ] \text{ and } U_N \triangleq [\ v_{n+1} \mid v_{n+2} \mid \ \ldots v_m\ ] \tag{3.13}$$

as defined before v_i is ith eigenvector of R. The noise subspace is orthogonal to the direction vectors. Expressing the projection of noise subspace onto the space spanned by direction vectors

$$Q_{MU}(z) = a^T(1/z)U_N U_N^H a(z) = a^T(1/z)(1 - U_S U_S^H)a(z) \tag{3.14}$$

$$Q_{MU}(z) = q_{-m+1}z^{-m+1} + \cdots + 0 \cdots + q_{m-1}z^{m-1} \tag{3.15}$$

has a conjugate symmetry property that is $q_{-m} = q_{-m}^*$. This polynomial has $2(m-1)$ roots, but roots come in conjugate symmetric pairs. Only one of the conjugate pair is chosen.

If the eigendecomposition corresponds to the true spectral matrix, then the exact MUSIC spectrum is obtained by evaluating $Q_{MU}(z)$ on the unit circle. Since $z = e^{j\psi}$ is in the array manifold vector in place of $g(\theta)$. These roots correspond to the locations of the n signals in the ψ domain. Denoting the roots by z_i for $i = 1,\ 2,\ \ldots\ , n$ then

$$\psi_i = arg(z_i) \text{ for } i = 1,\ 2,\ \ldots\ , n \tag{3.16}$$

The n DOA estimates of the root-MUSIC algorithm are found by a simple inverse function operation

$$\psi = g(\theta) = 2\pi d cos(\theta) \tag{3.17}$$

The values of the $g(\theta_i)$ giving ψ_i are the DOA estimates. Mathematically

$$\theta_i = g^-1(\psi_i) \text{ for } i = 1,\ 2,\ \ldots,\ n \tag{3.18}$$

$$\theta_i = acos(\frac{\psi_i}{2\pi d}) \text{ for } i = 1,\ 2,\ \ldots,\ n \tag{3.19}$$

In section 3.1 it is mentioned from the properties (3.9) and (3.10) which makes it possible to use the high resolution eigenstructure based algorithms. Another important property is about the function from which DOA estimates of root-MUSIC are found by a function inversion.

$$\theta_i = g^{-1}(\psi_i) \text{ for } i = 1,\ 2,\ \ldots,\ n \tag{3.20}$$

Actually invertibility of this function $g(\theta)$ is a key to success of the root-MUSIC algorithm. Actually any array which has an array manifold vector having Vandermonde structure with a $g(\theta)$ which is a mapping

$$g(\theta) : [0\ \ \pi] \longrightarrow [0\ \ \pi] \text{ and invertible} \tag{3.21}$$

with specified properties can be used to find DOA estimates with root-MUSIC. Second question which readily arises from this discussion is, if there is another real *physical* array structure which results in a $g(\theta)$ having mentioned properties. There is no real array positions having the necessary Vandermonde structure, however it is possible to use a virtual array having the necessary Vandermonde structure.

3.3 Spatial Smoothing

Eigenstructure-based techniques are known to be high resolution and asymptotically unbiased estimates even in the case that the sources are partially correlated. However when the sources are coherent, i.e. fully correlated these methods encounter difficulties. In section 3.1 the properties (3.9) and (3.10) are mentioned in detail which makes it possible to use the high resolution eigenstructure based algorithms . In this chapter, spatial smoothing preprocessing is reviewed. Assume for simplicity that only two sources are coherent $s_1(t)$ and $s_2(t)$. The coherence of sources can be mathematically expressed as

$$s_2(t) = \alpha s_1(t) \tag{3.22}$$

For coherence, i.e., fully correlated case $\alpha = \beta e^{(j\phi)}$

For this case writing (2.28) again

$$s(t) = \begin{pmatrix} (1+\alpha)s_1(t) & s_3(t) & \dots & s_n(t) \end{pmatrix}^T \tag{3.23}$$

where $s(t)$ is reduced to$n-1X1$ matrix and $A(\theta)$ is also reduced to $n-1Xm$ matrix

$$A(\theta) = \begin{pmatrix} a(\theta_1) + \alpha a(\theta_2) & a(\theta_3) & \dots & a(\theta_n) \end{pmatrix}^T \tag{3.24}$$

Now $S = E\{s(t)s(t)^H\}$, the covariance matrix of the modified signals is a $(n-1)X(n-1)$ *nonsingular* matrix and A is of full column rank. But in the nonmodified form it is *singular* with rank $n-1$. Again looking at the properties 1) and 2) for this case

1) the minimal eigenvalue of R is equal to σ^2 with multiplicity $(m-(n-1))$

2) the eigenvectors corresponding to the minimal eigenvalue are orthogonal to the columns of the A matrix, i.e. the direction vectors of the signals. But the columns of A in 2.28 is not linearly independent.

Since the signal subspace is spanned by $n-1$ direction vectors the number of detected signals will be $n-1$. In general if q out of the n signals are coherent the eigenstructure based method will detect $n-q$ signals giving DOA estimates of noncoherent sources. Spatial smoothing preprocessing technique is introduced by Evans *et al*, which deals with the nonsingularity of the covariance of the signals. The preprocessing technique is given to restore the nonsingularity of the signal covariance.

3.3.1 The Spatial Smoothing Preprocessing Technique

A linear uniformly spaced array with m elements, with element spacing d in terms of wavelength is divided into overlapping subarrays of size m_0. m_0 should be greater then the number of sources. From equation (1.22), the kth $k = 0,\ 1\ , \dots,\ K$ where $K = m + 1 - m_0$ subarray output datamodel is

written as

$$x_k(t) = A(\theta)D^{k-1}s(t) + n_k(t) \tag{3.25}$$

Where D symbolizes the nXn diagonal matrix and D^k stands for the kth power of the D matrix .

$$D = diag\{e^{jg(\theta_1)},\ e^{jg(\theta_2)}\ e^{jg(\theta_3)} \dots e^{jg(\theta_n)}\} \tag{3.26}$$

$$x_k(t) = A(\theta)D^{k-1}s(t) + n_k(t) \tag{3.27}$$

The data covariance matrix of the kth subarray equation is given by

$$R_k = E\{x_k(t)x_k(t)^H\} = AD^{k-1}SD^{k-1}A^H + {\sigma_n}^2 I \tag{3.28}$$

Then the spatially smoothed data covariance matrix is defined by

$$R^s = \frac{1}{K}\sum_{k=1}^{K} R_k \tag{3.29}$$

It is proven in reference [16], if the number of subarrays is greater than the number of coherent sources than the smoothed covariance matrix is nonsingular. R^s has the same form as R^s, so it can be successfully used with eigenstructure based methods. This technique is called forward spatial smoothing. Another technique which gives better results is given by Pillai in [20] called backward-forward smoothing. Where D_k^b symbolizes the nXn diagonal matrix

$$D_k^b = diag\{e^{-j(m_0+k-2)g(\theta_1)},\ e^{j(m_0+k-2)g(\theta_2)}\ e^{j(m_0+k-2)g(\theta_3)} \dots e^{j(m_0+k-2)g(\theta_n)}\} \tag{3.30}$$

$$R_k^b = AD_k^b S^* {D_k^b}^H A^H + {\sigma_n}^2 I \tag{3.31}$$

The backward smoothed data covariance matrix is calculated by

$$R^b = \frac{1}{K}\sum_{k=1}^{K} R_k \tag{3.32}$$

Forward-Backward smoothed data covariance matrix is obtained by averaging Forward and Backward smoothed covariance data matrix, i.e.,

$$R^{bf} = \frac{1}{2}(R^b + R^s) \tag{3.33}$$

In [20] Pillai proved that if there are n sources to be resolved, then independent of the number of coherent sources q $n/2$ subarray of length $m_0 = m + 1 - n/2$. The proof details are in [20].

CHAPTER 4

ARRAY INTERPOLATION:VIRTUAL ARRAY CONCEPT

In chapter 3, the formulization of root-MUSIC algorithm which is one of the eigenstructure based algorithms and spatial smoothing preprocessing technique for ULA's is given. The most restrictive aspect of high resolution eigenstructure based algorithms and spatial smoothing techniques is that they both require an ULA. Array interpolation is a subject which gives the opportunity to use these techniques for a general class of non-structured arrays. Array interpolation is a technique in which a virtual array is obtained from the real array and the outputs of the virtual array, computed from the real array using a linear transformation, is used for DOA estimation. In this chapter the concept of array interpolation is investigated. Two important array interpolation techniques, introduced to the litrature by Friedlander in [11] and Markus Bühren in [6] is explained. The differences of these two methods are given in detail in subsequent sections.

4.1 Virtual Array Design For Array Interpolation

In array interpolation, the main idea is to find an interpolation matrix B which will linearly transform the *real array* manifold onto a preliminary specified *virtual array* manifold over a given angular sector of the xy-plane.

In this section the design of interpolated array, i.e., virtual array is explained. The mathematical formulation of the two different array interpolation methods respectively introduced by Friedlander in [11] and Markus Bühren in [6] is given. This two methods differ in the method of choosing the virtual array manifold. In friedlander's method the virtual array is a physical virtual array which is a uniformly spaced linear array, i.e., in Friedlander's interpolation scheme [11] the original array is tried to be approximated by an ULA by placing the virtual array elements as close as the real array elements. However, in Markus Bühren [6] interpolation method the virtual array is not a physical virtual array. It has only the virtual array manifold vector having the necessary Vandermonde structure to use root-MUSIC and spatial smoothing preprocessing techniques.

In section 3.1, it is mentioned from the properties (3.9) and (3.10) which makes it possible to use the high resolution eigenstructure-based algorithms. Another important property is about the function from which DOA estimates of root-MUSIC are found by a function inversion.

$$\theta_i = g^{-1}(\psi_i) \text{ for } i = 1,\ 2,\ \ldots,\ n \tag{4.1}$$

The invertibility of this function $g(\theta)$ is a key to success of the root-MUSIC algorithm. Any array which has an array manifold vector having Vandermonde structure with a $g(\theta)$ which is a mapping

$$g(\theta) : [0\ \ \pi] \longrightarrow [0\ \ \pi] \text{ and invertible} \tag{4.2}$$

with specified properties and can be used to find DOA estimates with root-MUSIC. There is no other real array than ULA which results in such a $g(\theta)$. However Markus Bühren [6] introduces a method called virtual array design via differential geometries to find a virtual array manifold vector having the form and optimally matching the directional properties of the virtual array.

$$\psi = g(\theta) \text{ then } a(\theta) = e^{-j(\frac{(m-1)}{2})\psi} \begin{pmatrix} 1 & e^{j\psi} & e^{j2\psi} & \ldots & e^{j(m-1)\psi} \end{pmatrix}^T \tag{4.3}$$

4.1.1 Problem Formulation

Let an array of m randomly distributed sensors in the xy-plane with coordinates $p_n = (x_n \ y_n)^T$ receive n narrowband plane waves from far-field emitters with the same center frequency f_c from directions $\theta_1, \ \theta_2 \ \ldots \ , \theta_n$ respectively.

The output data model and array manifold vector equations are given in (2.22) and (3.5).

4.1.2 Virtual ULA

In this method the real array manifold is approximated by a virtual ULA manifold. The most critical aspect of virtual ULA design is the positioning of virtual ULA elements. The choise of the origin of virtual ULA and the sensor spacings d_0 of virtual ULA determine the design of virtual ULA. The optimal positioning of the virtual ULA elements is an open question. As a rule of thumb the virtual ULA element positions are choosen as close as possible to the real array elements. The total aperture is adjusted to be approximately the same as the real array aperture. After choosing virtual array elements, the following step-by-step description given in [11] is followed in order to find interpolation matrix.

1-)The first step is choosing the field of view of the array. The field of view of the array named Θ is choosen as $[0^o \ \ 180^o]$ or more narrower. The field of view will be divided into L sectors namely subsectors Θ_l. For example, if the field of view is $[0^o \ \ 180^o]$ it can be divided into $L = 6$ sector, each 30^o. The lth sector is defined by $[\theta_l^{(1)} \ \ \theta_l^{(2)}]$

2-)Next each sector is segmented into smaller parts in order to use in the design phase of the array interpolation matrix.

$$\Theta_l = \left(\ \theta_l^{(1)} \quad \theta_l^{(1)} + \Delta\theta \quad \theta_l^{(1)} + 2\Delta\theta \quad \ldots \quad \theta_l^{(2)} \ \right) \tag{4.4}$$

3-)Continue by computing array sterring vector of the original array in each subsector using Θ_l's

$$A_l = \begin{pmatrix} a(\theta_l^{(1)}) & a(\theta_l^{(1)} + \Delta\theta) & a(\theta_l^{(1)} + 2\Delta\theta) & \dots & a(\theta_l^{(2)}) \end{pmatrix}^T \tag{4.5}$$

4-)Since the decision of element locations of the virtual ULA is done, virtual ULA manifold at the subsector θ_l Θ_l's can be calculated

$$\tilde{A}_l = \begin{pmatrix} \tilde{a}(\theta_l^{(1)}) & \tilde{a}(\theta_l^{(1)} + \Delta\theta) & \tilde{a}(\theta_l^{(1)} + 2\Delta\theta) & \dots & \tilde{a}(\theta_l^{(2)}) \end{pmatrix}^T \tag{4.6}$$

In other words A_l is the response of the real array to signals from directions Θ_l, where $\tilde{A}_l$ is the response of the virtual ULA to signals from directions Θ_l.

5-)The basic assumption is that the array manifold of the virtual array is obtained by linear interpolation of the real array manifold in each sector Θ_l. That is, there exists a constant B matrix in each defined subsector named B_l satisfying the equation

$$B_l A_l \approx \tilde{A}_l \tag{4.7}$$

This is an approximate equality. The computation of B_l matrix is done by a least-squares optimization. The frobenius norm of the $B_l A_l - tilde A_l$ is found and optimized in the lest squares sense. Without giving the details of mathematical formulation in this thesis, the solution of this optimization problem is given by

$$B_l = \tilde{A}_l A_l^H (A_l A_l^H)^{-1} \tag{4.8}$$

The calculations of interpolation matrices in each sector is done only once in the design phase θ_l for $l = 0,\ 1,\ 2,\ \dots\ L$.

4.1.3 Direction Finding with Interpolated Array:Virtual ULA method

In the algorihm application, the incoming data vectors are left-multiplied by the interpolation matrix, i.e., $Bx(t) = \tilde{x}(t)$. So the covariance matrix

of the signals from the virtual array can be calculated from the covariance matrix of the real array as

$$\tilde{R} = BRB^H \tag{4.9}$$

from (4.10) follows that

$$\tilde{R} = BA(\theta)SA^HB^H(\theta) + {\sigma_n}^2BIB^H = \tilde{A}S\tilde{A}^H + {\sigma_n}^2\tilde{I} \tag{4.10}$$

The covariance matrix $\tilde{R}$ corresponds to the array manifold $\tilde{A}$ of a uniformly spaced linear array. Therefore, the root-MUSIC algorithm can be applied to the covariance matrix $\tilde{R}$. The application of the root-MUSIC algorithm is explained in section 3.2. The virtual array manifold vector has a form

$$\psi = g(\theta) = 2\pi d_o cos(\theta) \text{ then } a(\theta) = e^{-j(\frac{(m-1)}{2})\psi} \begin{pmatrix} 1 & e^{j\psi} & e^{j2\psi} & \dots & e^{j(m-1)\psi} \end{pmatrix}^T \tag{4.11}$$

where d_o is the virtual array element spacing. The roots of the equation are found

$$\psi_i = arg(z_i) \text{ for } i = 1,\ 2,\ \dots\ , n \tag{4.12}$$

and

$$\theta_i = acos(\frac{\psi_i}{2\pi d_o}) \text{ for } i = 1,\ 2,\ \dots,\ n \tag{4.13}$$

B matrix only for one subsector, DOA estimates, i.e., θ_is which are outside the interpolation sector are omitted.

4.1.4 Virtual Array Using Differential Geometry

In this method the real array manifold is approximated by a virtual array manifold which has the necessary Vandermonde structure amenable to spatial smoothing and eigenstructure based direction of arrival estimation methods. In this section, the arc length representation of the array manifold vector is introduced. Then, it is explained how the arc length concept is used for

the development of a virtual array manifold vector having the Vandermonde structure.

4.1.5 Arc Length Representation

For an array of m randomly distributed sensors in the xy-plane with coordinates $p_n = (x_n \ y_n)^T$ the output data model and array manifold vector equations are given in (2.22) and (2.14). Writing the array manifold vector

$$a(\theta) = \begin{pmatrix} e^{j2\pi(x_0 cos(\theta)+y_0 sin(\theta))} \\ e^{j2\pi(x_1 cos(\theta)+y_1 sin(\theta))} \\ e^{j2\pi(x_2 cos(\theta)+y_2 sin(\theta))} \\ \vdots \\ e^{j2\pi(x_{m-1} cos(\theta)+y_{m-1} sin(\theta))} \end{pmatrix} \tag{4.14}$$

$a(\theta)$ is a complex vector. Supposing that the sensor positions aren't changing, then this complex steering vector represents a parametric curve equation parameterized by θ in the n dimensional complex space. Actually it is really hard to have an imagination of this curve, since the dimension n can be large. As θ changes from θ_0 to $(\theta_0 + \delta\theta)$, it is moved from a point from another point on the curve represented by the steering vector in the n dimensional space. The arc length of the curve (the length of curve as it is moved from θ_0 to θ_1) from θ_0 to θ_1 is found by integrating the length of the rate of change of the steering vector. Expressing mathematically, if $\dot{a}(\theta) = \frac{da(\theta)}{d\theta}$ then the arclength $s(\theta)$ as the length of the curve from 0 to θ is found

$$s(\theta) = \int_0^\theta \sqrt{\dot{a}(v)^H \dot{a}(v)} dv = \int_0^\theta \|\dot{a}(v)\| dv \tag{4.15}$$

$\dot{s}(\theta) = \|\dot{a}(v)\|$ has a physical meaning considering the array structure. This expression will give idea about how well the array can seperate two closely spaced sources impinging on the array. The array gives more accurate

DOA estimates for sources impinging on the array from directions θ for which $\dot{s}(\theta)$ is relatively large and accuracy is low for sources from directions θ for which $\dot{s}(\theta)$ is relatively small.

The mathematical expression for $\dot{s}(\theta) = \|\dot{a}(v)\|$ is obtained for a randomly distributed array. For a general idea for the meaning of arc length, it is calculated for ULA and UCA (Uniform Circular Array) case.

$$a(\theta) = \begin{pmatrix} e^{j2\pi(x_0 cos(\theta)+y_0 sin(\theta))} \\ e^{j2\pi(x_1 cos(\theta)+y_1 sin(\theta))} \\ e^{j2\pi(x_2 cos(\theta)+y_2 sin(\theta))} \\ \vdots \\ e^{j2\pi(x_{m-1} cos(\theta)+y_{m-1} sin(\theta))} \end{pmatrix} \tag{4.16}$$

then I is mXm unity matrix

$$c = diag\{ \begin{pmatrix} j2\pi(-x_0 sin(\theta) + y_0 cos(\theta)) \\ j2\pi(-x_1 sin(\theta) + y_1 cos(\theta)) \\ j2\pi(-x_2 sin(\theta) + y_2 cos(\theta)) \\ \vdots \\ j2\pi(-x_{m-1} sin(\theta) + y_{m-1} cos(\theta)) \end{pmatrix} \} \tag{4.17}$$

$$\dot{a}(\theta) = ca(\theta) \tag{4.18}$$

$$\dot{s}(\theta) = 2\pi \sqrt{\sum_{i=0}^{m-1} \left(-x_i sin(\theta) + y_i cos(\theta)\right)^2} \tag{4.19}$$

The resulting norm of the derivative $\dot{s}(\theta)$ can easily be calculated for a ULA placed on x axis with array element spacing d in terms of wavelength. $x_i = id$ and $y_i = 0$

$$\dot{s}(\theta) = 2\pi \sqrt{\sum_{i=0}^{m-1} \left(id sin(\theta)\right)^2} = 2\pi d\mu |sin(\theta)| \text{ where } \mu = \sqrt{\sum_{i=0}^{m-1} i^2} \tag{4.20}$$

When $\theta = \pi/2$, $\dot{s}(\theta)$ takes its maximum value, when $\theta = 0$ or π, then $\dot{s}(\theta)$ takes its minimum value. This is one way of justification for the well known fact that the accuracy of DOA estimation is best in the main direction of an ULA. The arc length os ULA can be calculated as

$$s(\theta) = 2\pi d\mu(1 - cos(\theta)) \text{ for } \theta \in [0\ \pi] \tag{4.21}$$

As it is seen for ULA the rate varies in a sinusoidal manner. Calculating for UCA with radius r in terms of wavelength. $x_i = rcos(\frac{2\pi}{m}i)$ and $y_i = rsin(\frac{2\pi}{m}i)$ then

$$\dot{s}(\theta) = 2\pi r\sqrt{\sum_{i=0}^{m-1}(sin(\frac{2\pi}{m}i - \theta))^2} = 2\pi r\sqrt{\frac{m}{2}} \tag{4.22}$$

$$s(\theta) = 2\pi r\sqrt{\frac{m}{2}}\theta \text{ for } \theta \in [0\ \pi] \tag{4.23}$$

When the array is UCA the rate of change of the array sterring vector is constant.

After giving the meaning and the formulation to find the arc length of array steering vector, the main intention is to find a virtual array manifold that has a Vandermonde structure also having the same directional behavior as the original array. An array manifold vector having the necessary Vandermonde structure can be constructed by finding $g(\theta)$ such that

$$\tilde{a}(\theta) = \begin{pmatrix} 1 & e^{jg(\theta)} & e^{j2g(\theta)} & \dots & e^{j(\tilde{m}-1)g(\theta)} \end{pmatrix}^T \tag{4.24}$$

where $\tilde{m}$ is the number of virtual array elements. The necessary conditions on a valid $g(\theta)$ is given on (3.21). The original array's directional behavior can be preserved by equating the virtual array's norm of change of rate and the real arrays norm of change of rate. That is

$$\dot{\tilde{s}}(\theta) = \dot{s}(\theta) \tag{4.25}$$

With the same mathematical formulation as above norm of the change of rate of $\tilde{a}(\theta)$ can be calculated as

$$\dot{\tilde{s}}(\theta) = \sqrt{\sum_{i=0}^{\tilde{m}-1} \dot{g}(\theta)^2} = \tilde{\mu}|\dot{g}(\theta)| \text{ where } \tilde{\mu} = \sqrt{\sum_{i=0}^{\tilde{m}-1} i^2} \tag{4.26}$$

$$\tilde{\mu}|\dot{g}(\theta)| = \dot{s}(\theta) \tag{4.27}$$

It is known that in order to use $g(\theta)$ in the root-MUSIC algorithm, a $g(\theta)$ function should be found which is a mapping

$$g(\theta) : [0 \;\; \pi] \longrightarrow [0 \;\; \pi] \text{ and invertible} \tag{4.28}$$

Invertibility implies, $g(\theta)$ should be monotonically increasing or monotonically decreasing, i.e.,

$$\dot{g}(\theta) > 0 \text{ or } \; < 0 \text{ for } \theta \in [0 \;\; \pi] \tag{4.29}$$

There is a freedom to choose $\dot{g}(\theta) > 0$ then the above equation turns out

$$\dot{g}(\theta) = \frac{\dot{s}(\theta)}{\tilde{\mu}} = \frac{\|\dot{a}(\theta)\|}{\tilde{\mu}} \tag{4.30}$$

and

$$g(\theta) = \frac{\dot{s}(\theta)}{\tilde{\mu}} = \frac{\|\dot{a}(\theta)\|}{\tilde{\mu}} \tag{4.31}$$

$$g(\theta) = \int_0^\theta \frac{\|\dot{a}(v)\|}{\tilde{\mu}} dv \tag{4.32}$$

This function satisfies $\dot{s}(\theta) = \dot{\tilde{s}}(\theta)$, meaning the directional behaviors of original real array is preserved. $g(\theta)$ is found by integrating a norm function. A norm function takes always positive or zero values. That's why the function $g(\theta)$ is a monotonically increasing function, implying invertibility. It is differentiable. Smoothness is a necessary condition for differentiability, so $g(\theta)$ is a smooth function.

A general procedure to find virtual array manifold can be given as follows:

1-)The first step is choosing the field of view of the array. The field of view of the array named Θ could be choosen as $[0^o \;\; 180^o]$ or more narrower.The field of view will be divided into L sectors namely subsectors Θ_l. For example, if the field of view is $[0^o \;\; 180^o]$ it can be divided into $L = 6$ sector, each 30^o. The lth sector is defined by $[\theta_l^{(1)} \;\; \theta_l^{(2)}]$

2-)Next each sector is segmented into smaller parts in order to use in the design phase of the array interpolation matrix.

$$\Theta_l = \begin{pmatrix} \theta_l^{(1)} & \theta_l^{(1)} + \Delta\theta & \theta_l^{(1)} + 2\Delta\theta & \dots & \theta_l^{(2)} \end{pmatrix} \tag{4.33}$$

3-)Continue by computing array sterring vector of the original array in each subsector using Θ_l's

$$A_l = \begin{pmatrix} a(\theta_l^{(1)}) & a(\theta_l^{(1)} + \Delta\theta) & a(\theta_l^{(1)} + 2\Delta\theta) & \dots & a(\theta_l^{(2)}) \end{pmatrix}^T \tag{4.34}$$

4-) $g(\theta)$ of the virtual array is calculated by discrete integration of the real array manifold rate of change norm. Thus, $\tilde{A}_l$ for each subsector Θ_l is calculated.

$$\tilde{A}_l = \begin{pmatrix} \tilde{a}(\theta_l^{(1)}) & \tilde{a}(\theta_l^{(1)} + \Delta\theta) & \tilde{a}(\theta_l^{(1)} + 2\Delta\theta) & \dots & \tilde{a}(\theta_l^{(2)}) \end{pmatrix}^T \tag{4.35}$$

5-)As in the ULA case, an interpolation matrix B_l satisfying the equation

$$B_l A_l \approx \tilde{A}_l \tag{4.36}$$

is found. As in the virtual ULA case, this is an approximate equality. The computation of B_l matrix is done by a least-squares optimization. The frobenius norm of the $B_l A_l - \tilde{A}_l$ is taken and optimized in the lest squares sense. Without giving the details of mathematical formulation in the thesis, the solution of this optimization problem is given by

$$B_l = \tilde{A}_l A_l^H (A_l A_l^H)^{-1} \tag{4.37}$$

These calculations are done for all subsector θ_l for $l = 0,\ 1,\ 2, \ldots, L$. This calculation of high computational effort has to be done only once in the design phase.

4.1.6 Direction Finding with Interpolated Array:Virtual Array Case

The root-MUSIC algorithm can be applied to the covariance matrix $\tilde{R}$. So,the array manifold vector have the necessary Vandermonde structure .The application of the root-MUSIC algorithm is the same in section 3.2. DOA's of the sources can be found by denoting the roots by z_i for $i = 1,\ 2,\ ....\ , n$ then

$$\psi_i = arg(z_i) \text{ for } i = 1,\ 2,\ ....\ , n \tag{4.38}$$

The n DOA estimates of the root-MUSIC algorithm are found by a simple inverse function operation. Again the DOA estimates are valid which fall in the interpolation sector. The values of the $g(\theta_i)$ giving ψ_i are the DOA estimates. Mathematically

$$\theta_i = g^{-1}(\psi_i)\ for\ i = 1,\ 2,\ \ldots,\ n \tag{4.39}$$

While this function can be easily calculated analytically, the inverse cannot be easily calculated by finding a functional representation as in the ULA case. Thus, representing the function by second order or third order splines is a reasonable approach. The interpolation error for finding the reverse function directly will be in direction of arrival estimation error. However, this is a deterministic error. If small intervals are choosen for spline interpolation then this error is negligible compared to the stochastic error in DOA estimation.

4.2 Interpolated Spatial Smoothing

The spatial preprocessing technique is amenable to all arrays having the necessary Vandermonde structure. The array manifold vector of the virtual array have the necessary Vandermonde structure. This means spatial smoothing technique can be readily used. The discussion is given for the general case in section 2.3.1 for an array manifold vector having necessary Vandermonde structure.

CHAPTER 5

Simulation Results

In this section, the results of the several simulated experiments with different scenarios are presented. The simulated experiments are performed for one, two ,three and four sources. In the first part of the simulations, the sources are uncorrelated and the simulations are performed in order to explore the performances of the two interpolation methods. The parameters affecting the interpolation quality are discussed. In the second part of the simulations, the sources are correlated and the simulations are performed in order to explore the performance of the interpolated spatial smoothing algorithm applied with the two interpolation methods. In all of the simulations, the performances are evaluated in the sense of root mean squared error and they are compared with the stochastic Cramer-Rao lower bound (CRB) [13] calculated theoretically for the original array.

For the simulations, an arbitrary array geometry of N=13 sensors depicted in Figure 5.1 is used. By applying the two interpolation methods to the real array geometry two different interpolation matrices are obtained. Interpolated root-MUSIC algorithm is used for the DOA estimation. It is assumed that 1000 snapshots are available for processing and 500 simulation runs are performed per point. For the interpolated spatial smoothing performance analysis correlated sources are generated with different correlation coefficients.

5.1 Uncorrelated Sources

In this section, the results of the simulations are presented for the performance evaluation of the two interpolation methods in the sense of root mean squared error by using the interpolated root-MUSIC algorithm. The simulations are performed for one, two and three sources. The parameters affecting the interpolation quality are explored.

5.1.1 One Source

In the simulations, one source is created and its DOA angle is swept from 0^o to 180^o. Firstly, the interpolation sector is taken as $[0^o\ 180^o]$. The interpolation sector and the positions of the array elements are seen in Figure 5.2. RMSE versus source DOA angle is plotted for the three SNR levels. In Figure 5.5 RMSE versus source DOA angle is seen for 10 dB. The SNR level is changed to 30 dB and the RMSE versus source DOA angle is plotted. The result is seen in Figure 5.4. In order to explore the bias caused by the interpolation error, the SNR level is changed to 60 dB and the RMSE versus source DOA angle is plotted. The result is seen in Figure 5.3.

In order to see the sector width effect on the interpolation error the interpolation sector is taken as $[45^o\ 72^o]$. The interpolation sector and the positions of the array elements are seen in Figure 5.6. The same simulations are performed with one source whose DOA angle is swept from 0^o to 180^o and RMSE versus source DOA angle for the three different SNR levels. In Figure 5.9 the plot for 10 dB is seen. In Figure 5.8 the plot for 30 dB is seen and In figure 5.7 the plot for 60 dB is seen.

From the simulations, it is concluded that as the interpolation sector gets narrower RMSE decreases. This is due to the fact that for the broad interpolation sector the estimates are highly biased, i.e. the quality of the interpolation is low. For broad interpolation case, estimation error is primar-

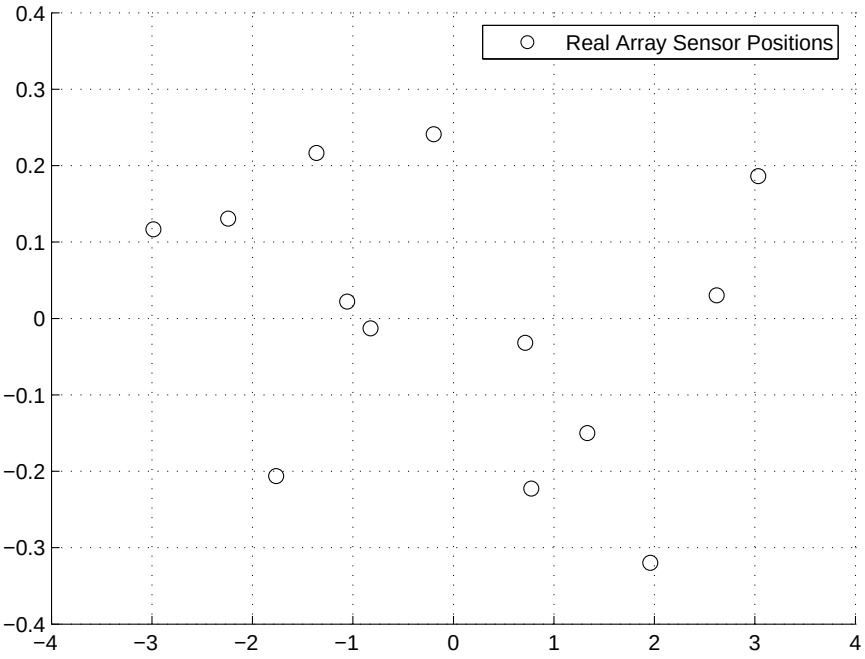

Figure 5.1: Real array element positions

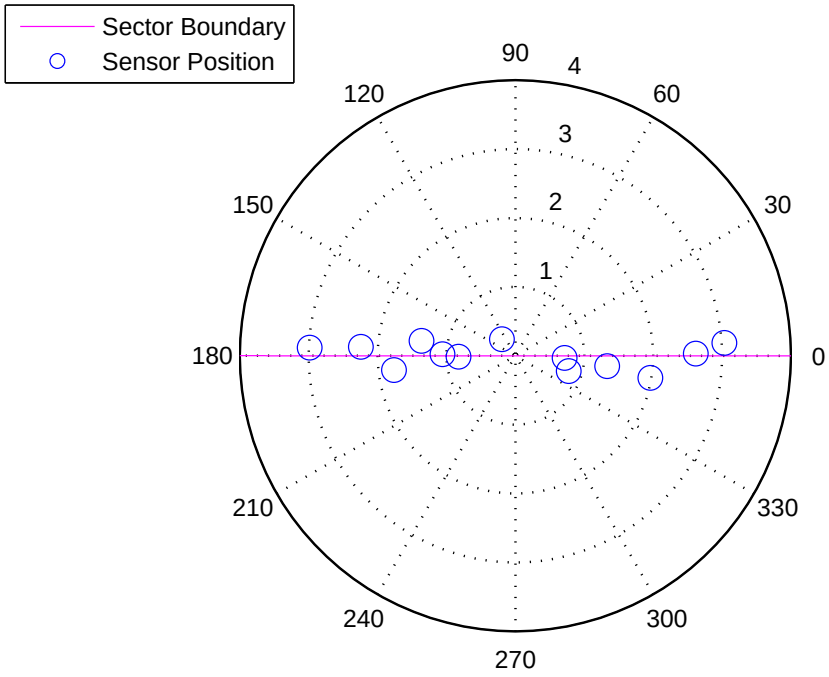

Figure 5.2: The interpolation sector and real array element positions

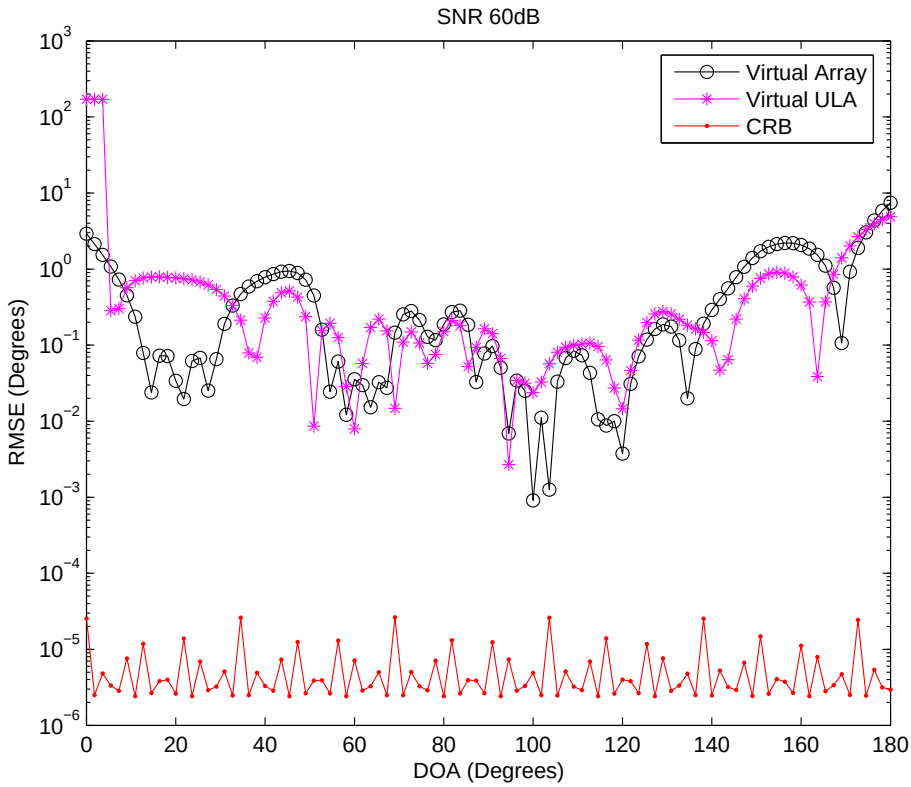

Figure 5.3: Performances of two interpolation methods and comparison with CRB of the original array when the source DOA angle is changing from 0^o to 180^o degrees. (Interpolation sector is $[0^o\ 180^o]$ degrees. SNR 60 dB)

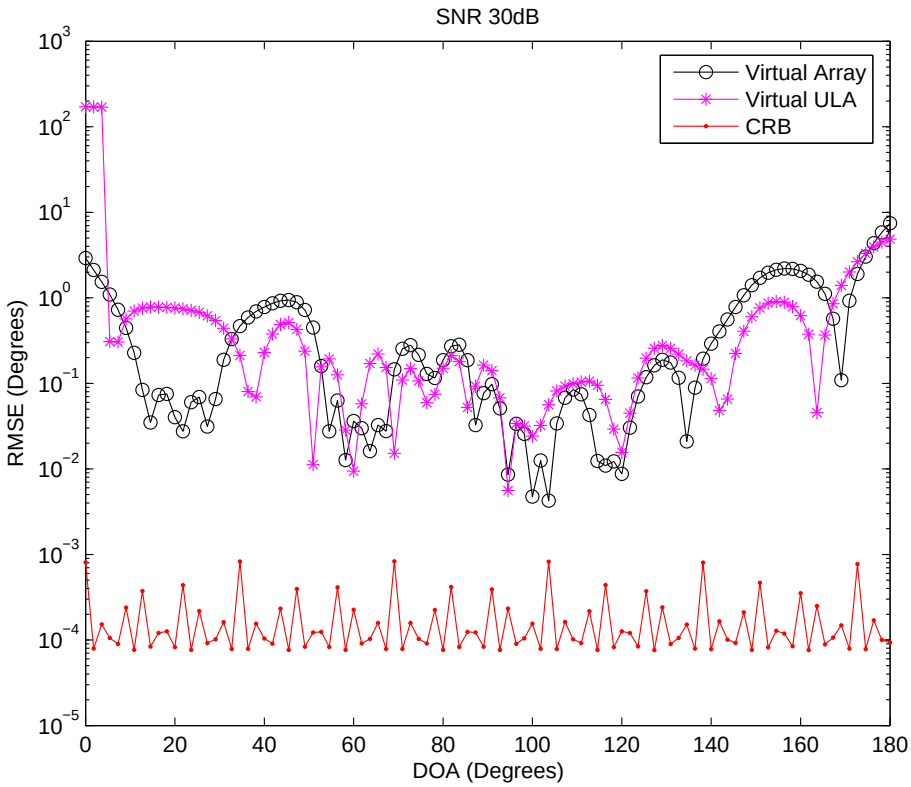

Figure 5.4: Performances of two interpolation methods and comparison with CRB of the original array when the source DOA angle is changing from 0^o to 180^o degrees. (Interpolation sector is $[0^o\ 180^o]$ degrees. SNR 30 dB)

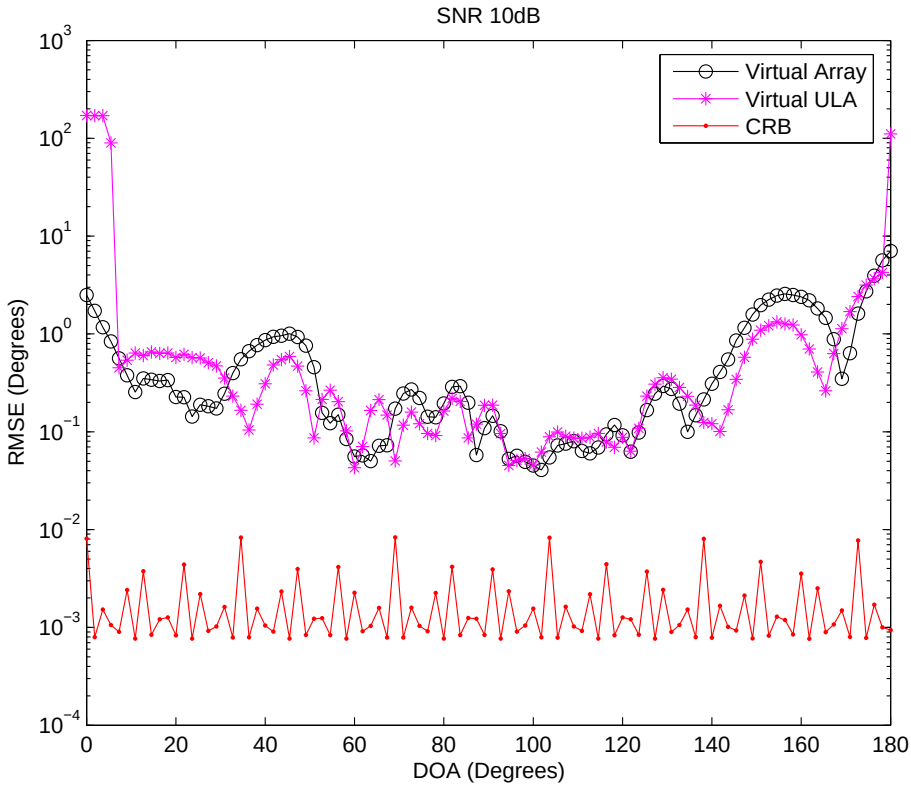

Figure 5.5: Performances of two interpolation methods and comparison with CRB of the original array when the source DOA angle is changing from 0^o to 180^o degrees. (Interpolation sector is $[0^o\ 180^o]$ degrees. SNR 10 dB)

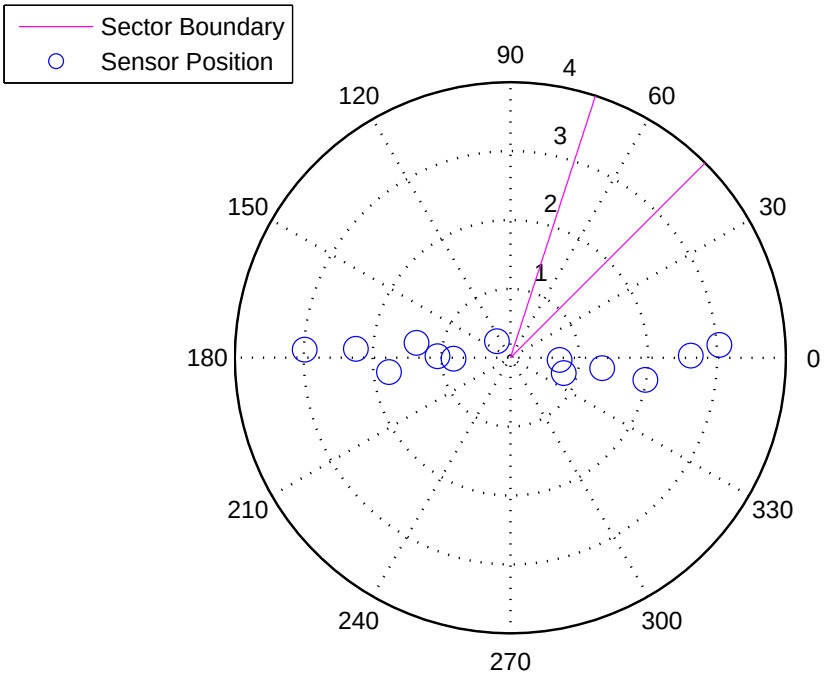

Figure 5.6: The interpolation sector and real array element positions

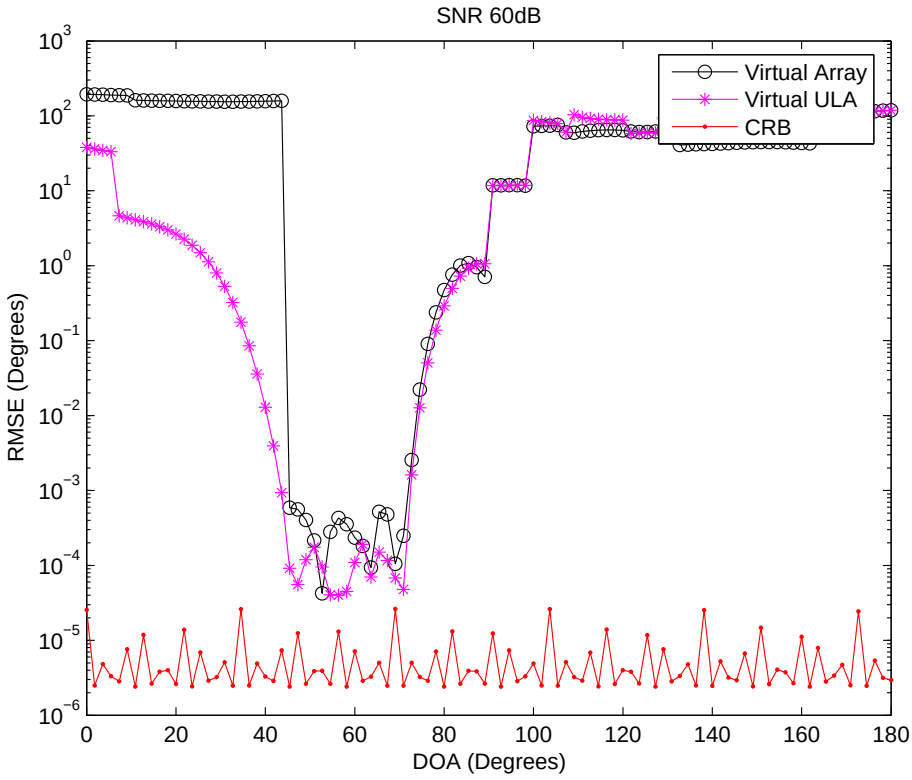

Figure 5.7: Performances of two interpolation methods and comparison with CRB of the original array when the source DOA angle is changing from 0^o to 180^o degrees. (Interpolation sector is $[45^o\ 72^o]$ degrees. SNR 60 dB)

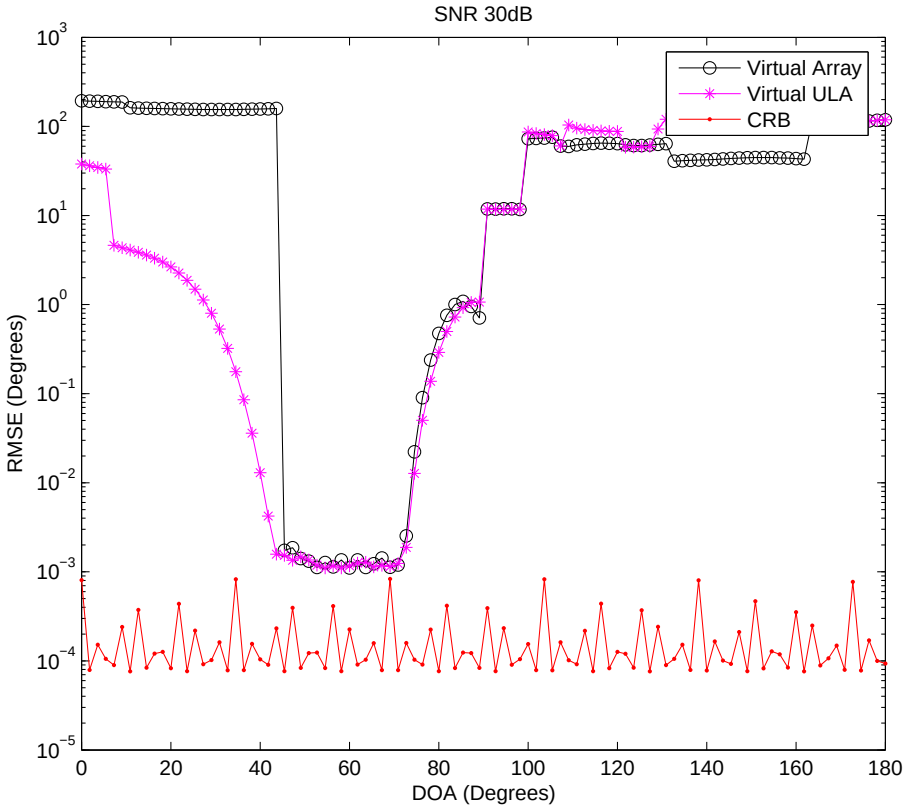

Figure 5.8: Performances of two interpolation methods and comparison with CRB of the original array when the source DOA angle is changing from 0^o to 180^o degrees. (Interpolation sector is $[45^o\ 72^o]$ degrees. SNR 30 dB)

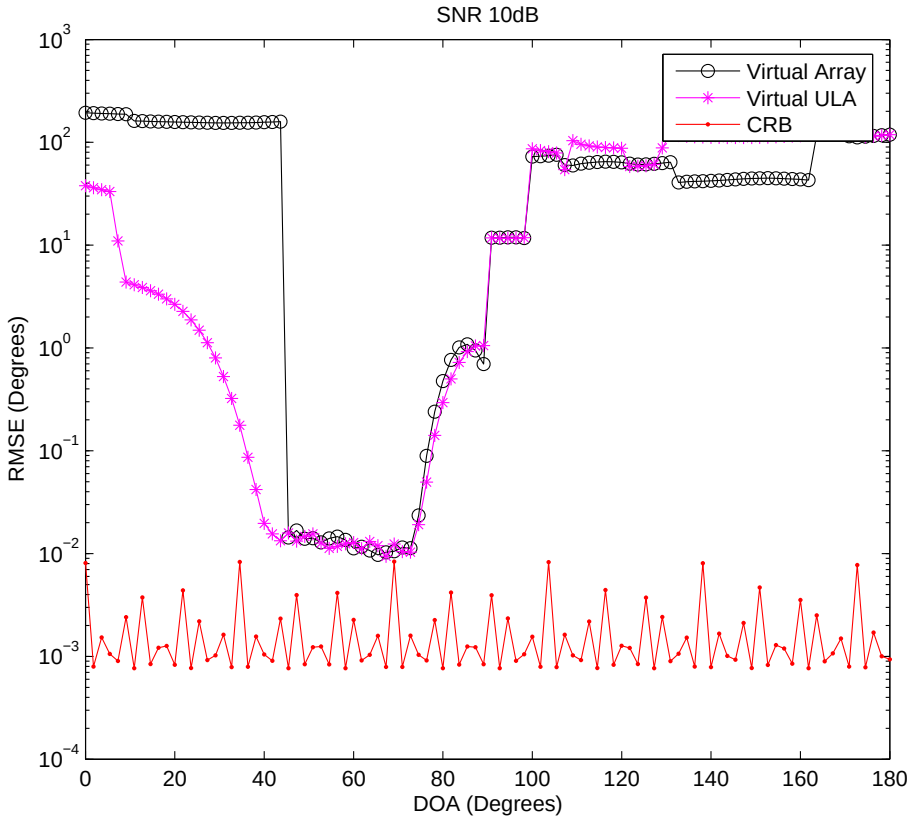

Figure 5.9: Performances of two interpolation methods and comparison with CRB of the original array when the source DOA angle is changing from 0^o to 180^o degrees. (Interpolation sector is $[45^o\ 72^o]$ degrees. SNR 10 dB)

ily caused by interpolation errors, SNR effect is small. However, for narrow interpolation sector the primary cause of the estimation error is SNR. The stochastic CRB is a meaningful measure when interpolation sector is sufficiently narrow, so that the quality of the interpolation is high.

Another important criterion for the RMSE to be close to the stochastic CRB is the number of snapshots. It should be large enough. In Figures 5.10 and 5.11 the number of snapshots available is 100 and 1000 respectively and the interpolation sector is taken as $[88^o\ 93^o]$. The interpolation sector and the positions of the array elements are seen in Figure 5.16. It is obvious that as the number of snapshots increase the RMSE gets closer to the CRB. "It is known that CRB provides a good measure of actual performance under small error conditions. Under large error conditions, i.e. low SNR or small number of snapshots the CRB values are overly optimistic." [11].

In [12], it is stated that the accuracy of the interpolator is determined by the frobenius norm $B_l A_l - \tilde{A}_l$ ratio to the norm of A_l. If the ratio of the error norm to the array manifold vector norm is small enough and the interpolator design can be accepted. In Figure 5.12 the frobenius norm ratio versus interpolation sector plot is seen.

The interpolation matrix should be well conditioned in order that the design is acceptable. In Figure 5.13 condition number versus interpolation sector plot is seen. By looking at the condition number versus interpolation sector width plot, the designer can choose the minimum sector width for which the condition number is acceptable before starting to design the interpolator. It should be noted that as the interpolation sector gets narrower the frobenius ratio rapidly decreases. However, the interpolation matrix becomes nonsingular. There is a tradeoff between the condition number of the interpolation matrix and the frobenius norm ratio.

Some simulations are done in order to see the effect of interpolation sector partition on the interpolation quality. The interpolation sector width is

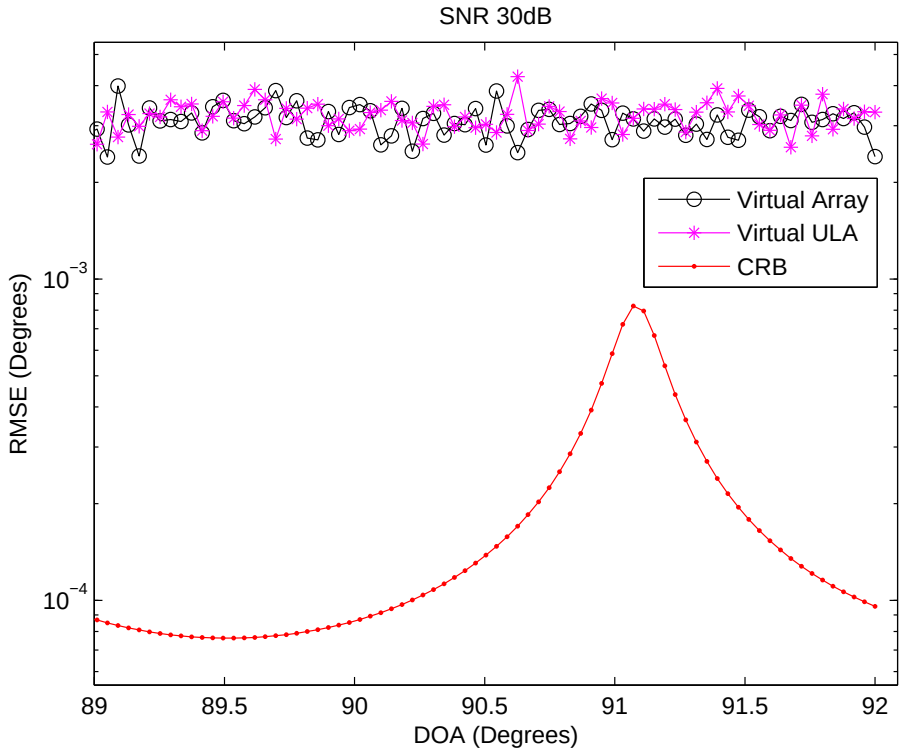

Figure 5.10: Number of snapshot effect. Source DOA angle is changing from 88^o to 93^o degrees. (Interpolation sector is [88^o 93^o] degrees). SNR 30 dB. Number of snapshots 100

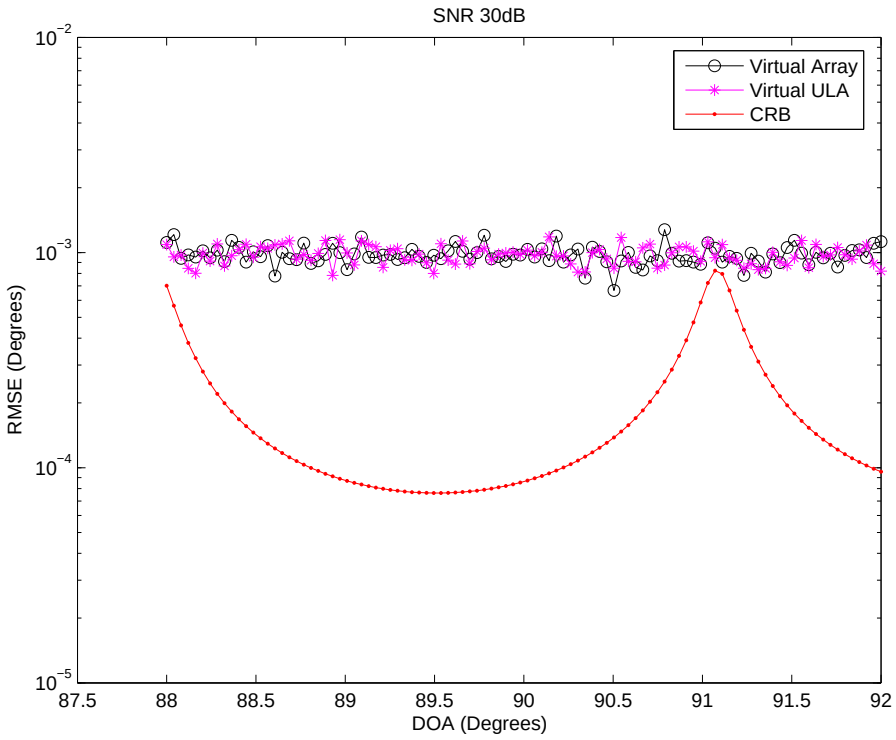

Figure 5.11: Number of snapshot effect. Source DOA angle is changing from 88^o to 93^o degrees. (Interpolation sector is[88^o 93^o] degrees). SNR 30 dB. Number of snapshots 1000

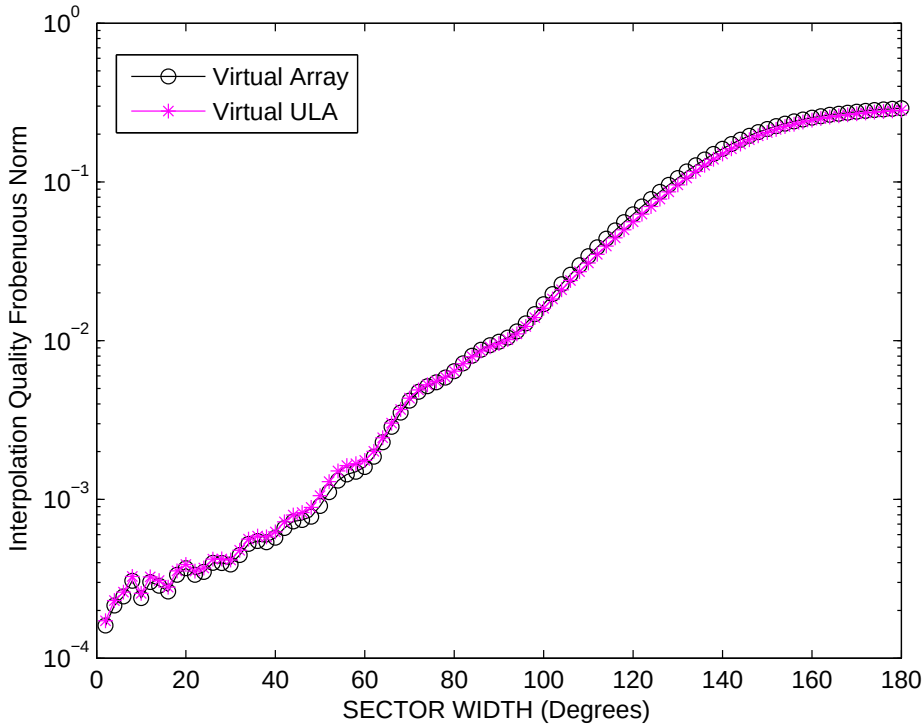

Figure 5.12: Frobenius norm ratio versus interpolation sector width

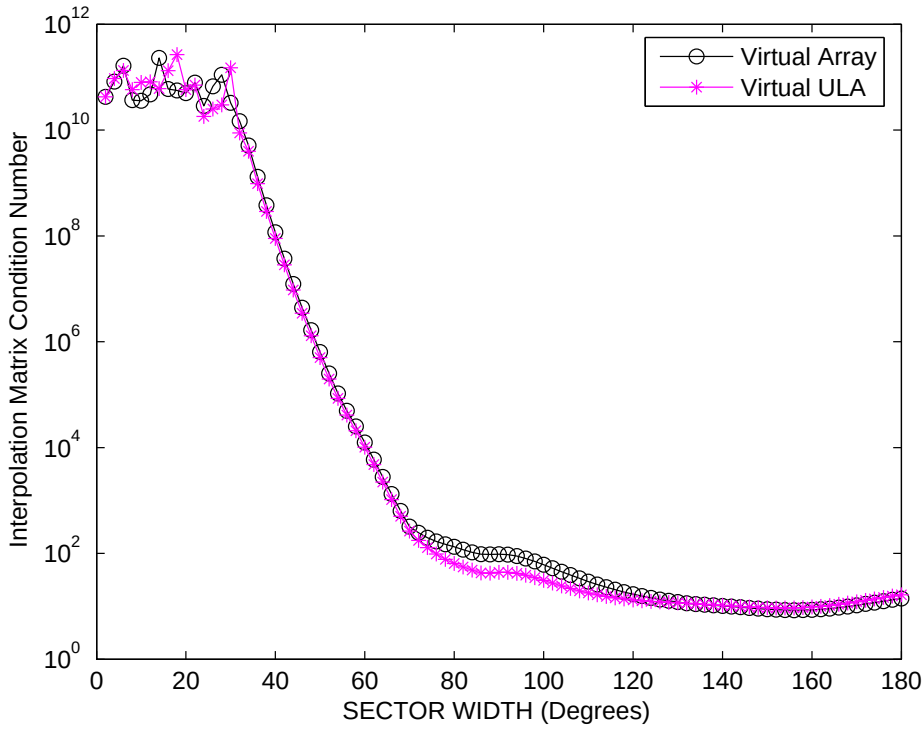

Figure 5.13: Interpolation matrix condition number versus interpolation sector width

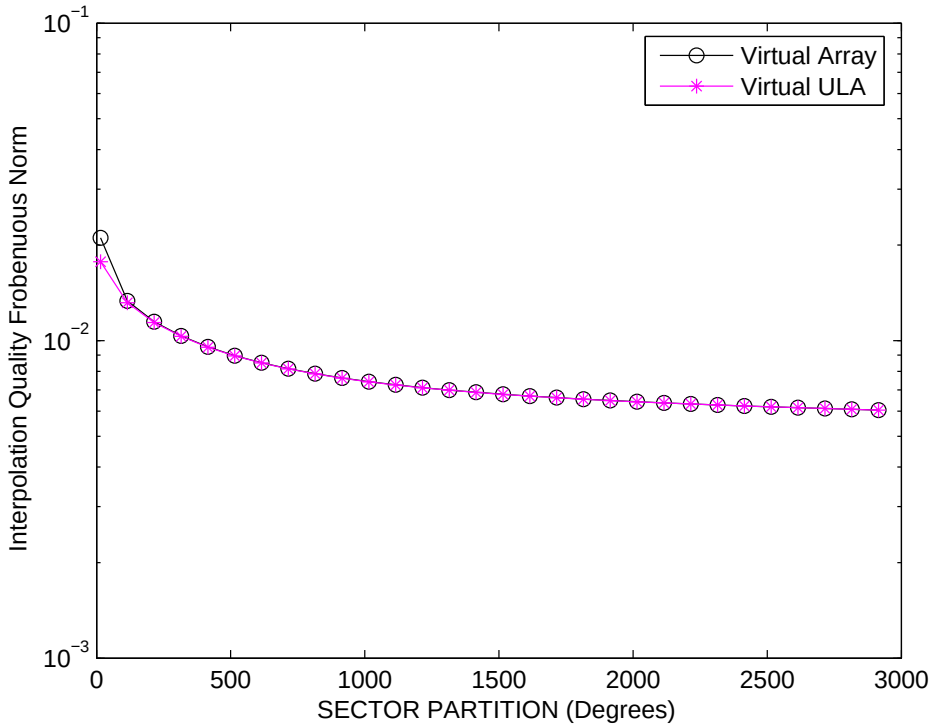

Figure 5.14: Frobenius norm ratio versus interpolation sector partition

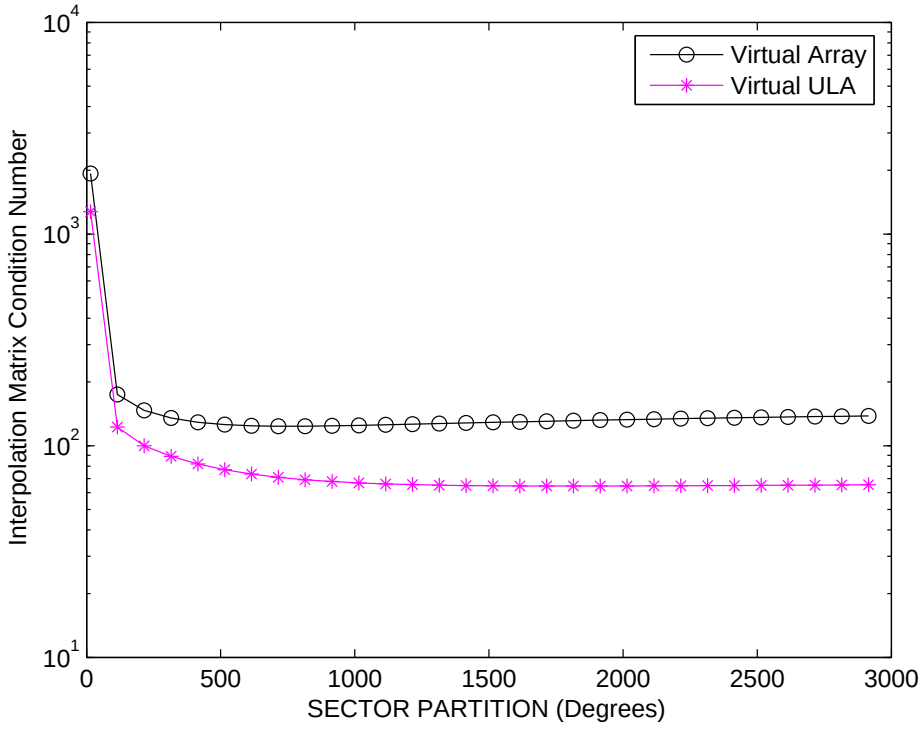

Figure 5.15: Interpolation matrix condition number versus interpolation sector partition

choosen as 80^o and the sector partition is changed from 15 to 3000. In Figure 5.14 the sector partition versus interpolation matrix condition number plot is seen. It is concluded from the Figure that as the sector partition gets larger, the condition number decreases. However, after some value the effect is not very obvious. In Figure 5.15 the sector partition versus frobenius norm ratio plot is seen. As the sector partition gets larger, the frobenius ratio decreases. However, after some value the effect is not very obvious. There is an optimum sector partition value considering both the condition number and frobenius norm. The designer can choose the optimum sector partition value by plotting these Figures, before starting the interpolator design.

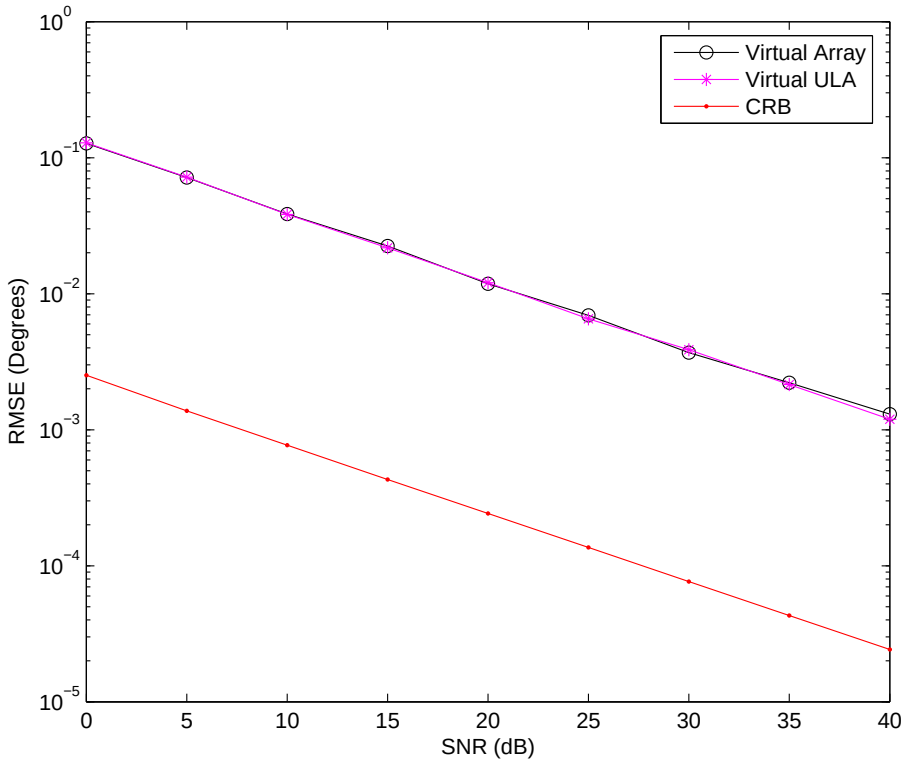

Figure 5.16: Performances of two interpolation methods compared with CRB for one source with DOA angle 58^o. (Interpolation sector $[45^o\ 72^o]$).

One source at fixed DOA angle is created at 58^o. SNR level is changed from 0 dB to 40 dB. The interpolation sector for this simulation is chosen as $[45^o\ 72^o]$. The DOA estimation RMSE versus SNR is plotted and compared with the stochastic CRB for the two interpolation methods. . The result is seen in Figure 5.16. As it is seen from the Figure the performances of two interpolation methods are the same. In Figure 5.17 the same performance curve is obtained for the interpolation sector $[0^o\ 180^o]$. The interpolation sector effect is obvious.

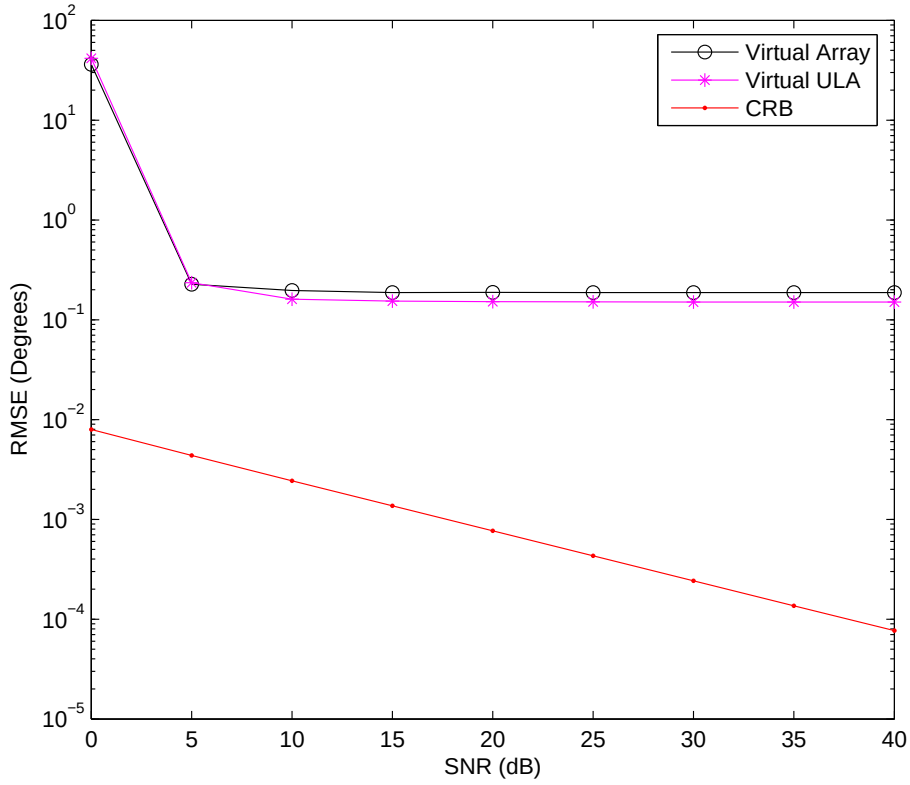

Figure 5.17: Performances of two interpolation methods compared with CRB for one source with DOA angle 58^o. (Interpolation sector $[0^o\ 180^o]$).

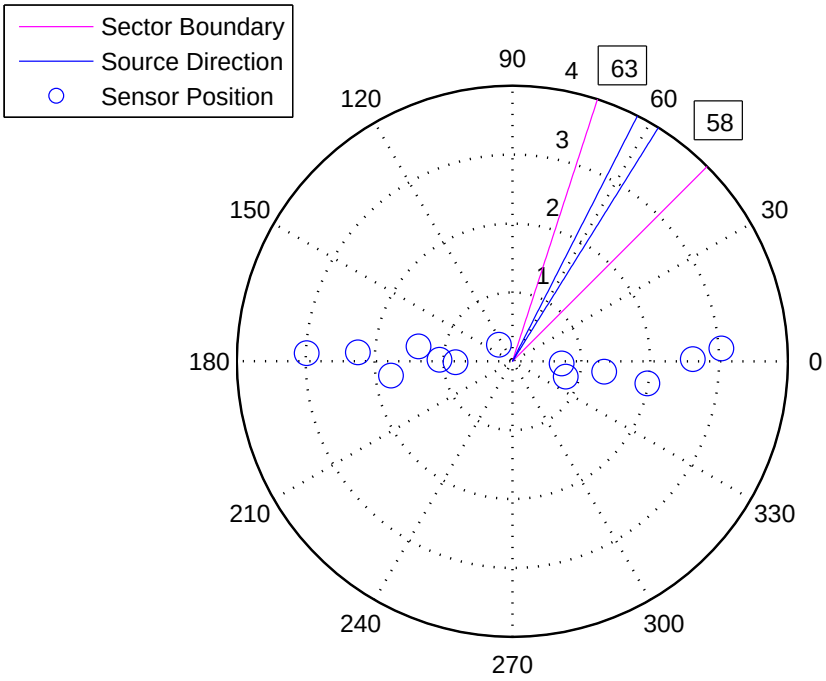

Figure 5.18: The interpolation sector and the sources impinging on the real array

5.1.2 Two Sources

Two equipower sources are created at fixed DOA angles 58^o and 63^o. SNR level is changed from 0 dB to 40 dB. The interpolation sector for this simulation is chosen as $[45^o\ 72^o]$. The interpolation sector and the sources impinging on the array elements are seen in Figure 5.18. The DOA estimation RMSE versus SNR is plotted and compared with the stochastic CRB for the two interpolation methods.

In Figure 5.19 DOA estimation RMSE for the two interpolation methods versus SNR compared with stochastic CRB is shown.

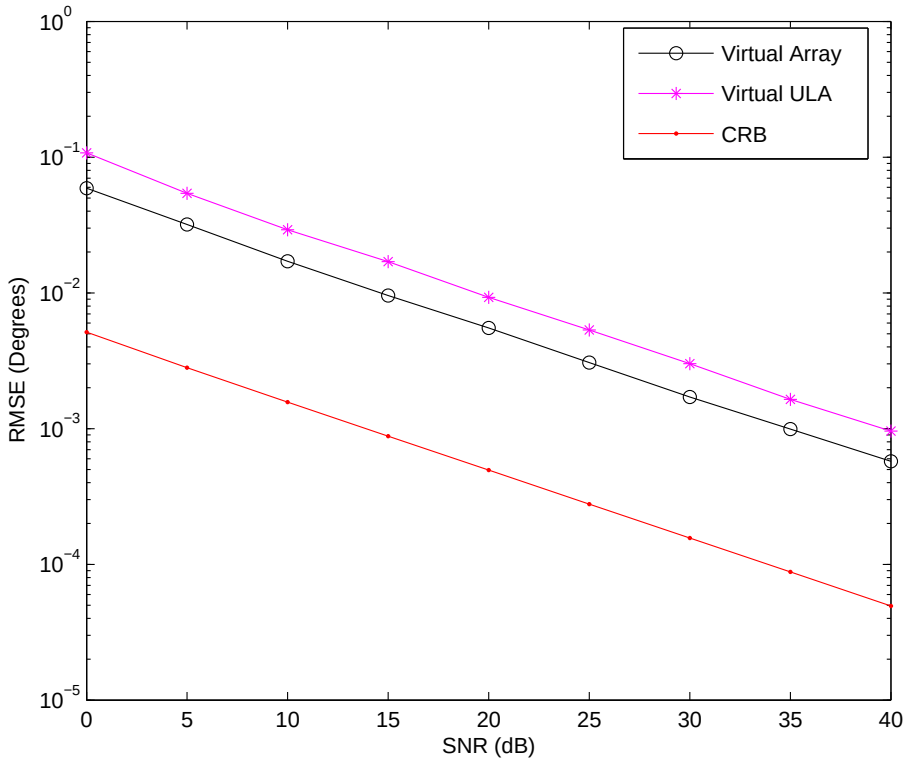

Figure 5.19: Performances of two interpolation methods compared with CRB for two equipower uncorrelated sources with DOA angles 58^o and 63^o. (Interpolation sector $[45^o\ 72^o]$).

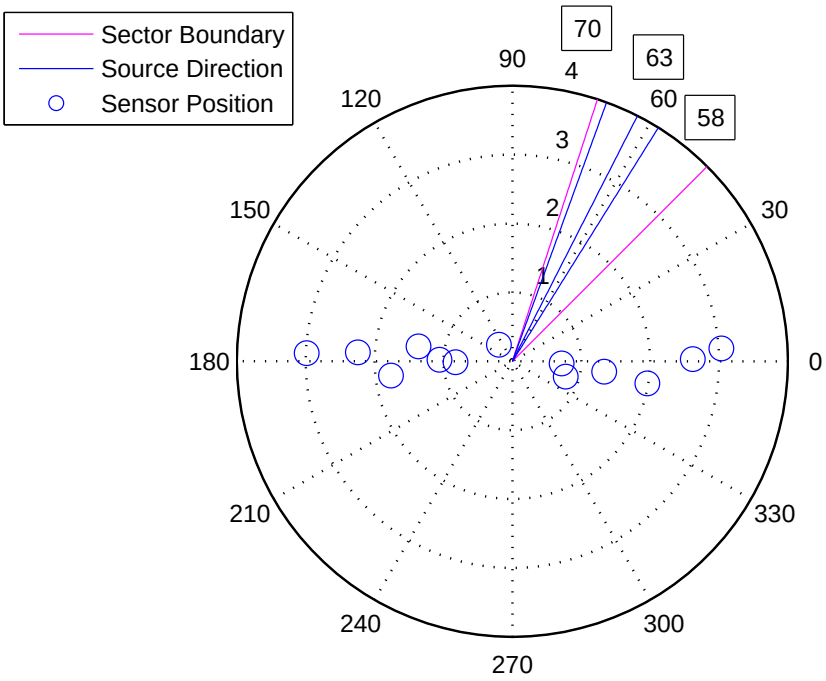

Figure 5.20: The interpolation sector and the sources impinging on the real array

5.1.3 Three Sources

Three equipower sources are created at fixed DOA angles 58^o, 63^o and 70^o. SNR level is changed from 0 dB to 40 dB. The interpolation sector for this simulation is chosen as $[45^o\ 72^o]$. The interpolation sector and the sources impinging on the array elements are seen in Figure 5.20. The DOA estimation RMSE versus SNR is plotted and compared with the stochastic CRB for the two interpolation methods.

In Figure 5.21 DOA estimation RMSE for the two interpolation methods versus SNR compared with stochastic CRB is shown.

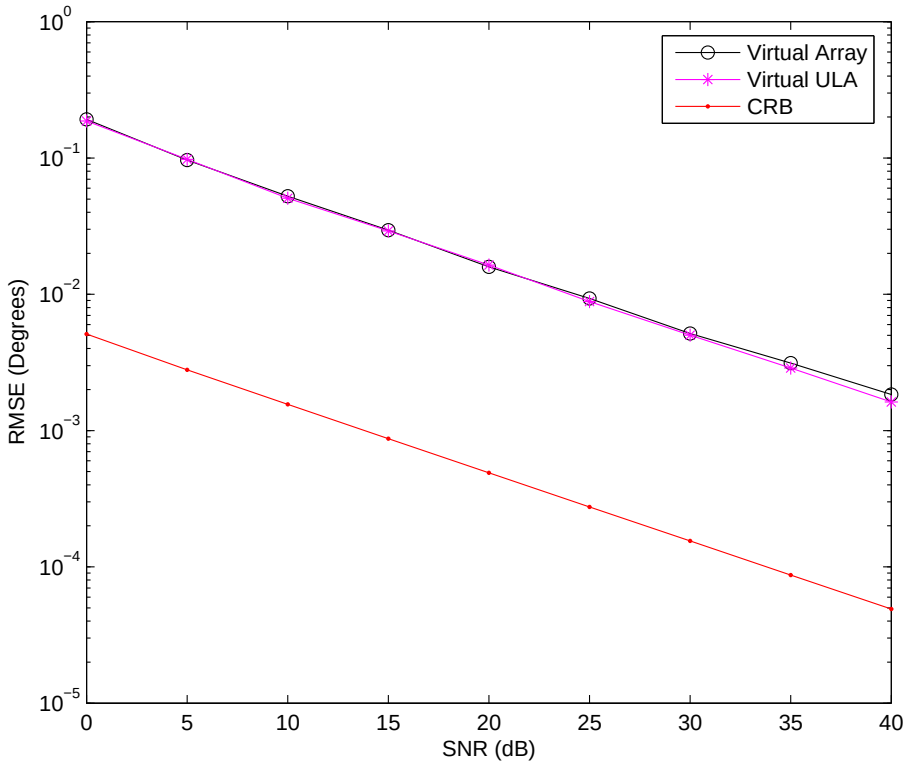

Figure 5.21: Performances of two interpolation methods compared with CRB for three equipower uncorrelated sources with DOA angles 58^o, 63^o and 70^o .(Interpolation sector $[45^o\ 72^o]$).

5.2 Interpolated Spatial Smoothing

In this section the results of the simulations for the correlated sources are presented. The simulations are performed in order to explore the performance of the interpolated spatial smoothing algorithm applied with the two interpolation methods. In all of the simulations, the performances are evaluated in the sense of root mean squared error and they are compared with the stochastic Cramer-Rao lower bound (CRB) [13] calculated theoretically for the original array. The experiments are performed for two, three and four sources.

5.2.1 Two Sources

Two equipower sources are created at fixed DOA angles 58^o and 63^o. The sources are correlated with correlation coefficient $\alpha = 0.7391$ and $\beta = 0.3061$. SNR level is changed from 0 dB to 40 dB. The interpolation sector for this simulation is chosen as $[45^o\ 72^o]$. The interpolation sector and the sources impinging on the array elements are seen in figure 5.22. The DOA estimation RMSE versus SNR is plotted and compared with the stochastic CRB for the two interpolation methods.

In Figure 5.23 DOA estimation RMSE for the two interpolation methods versus SNR compared with stochastic CRB is shown.

5.2.2 Three Sources

Three equipower sources are created at fixed DOA angles 45^o, 60^o and 115^o and two of them are correlated with correlation coefficient $\alpha = 0.4, -0.3$ and $\beta = 0.8, -0.7$. SNR level is changed from 0 dB to 40 dB. The interpolation sector for this simulation is chosen as $[20^o\ 120^o]$. The interpolation sector and the sources impinging on the array elements are seen in Figure

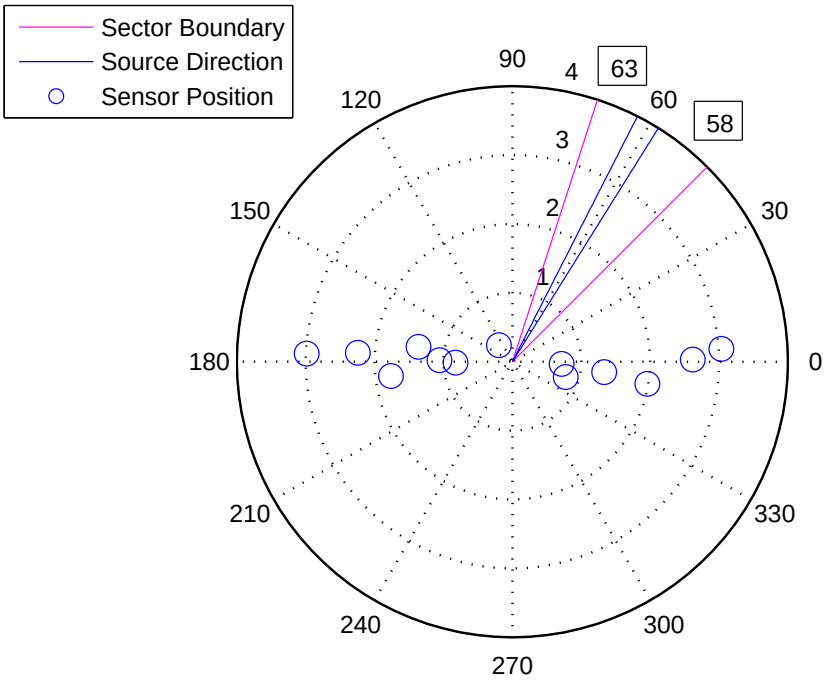

Figure 5.22: The interpolation sector and the sources impinging on the real array

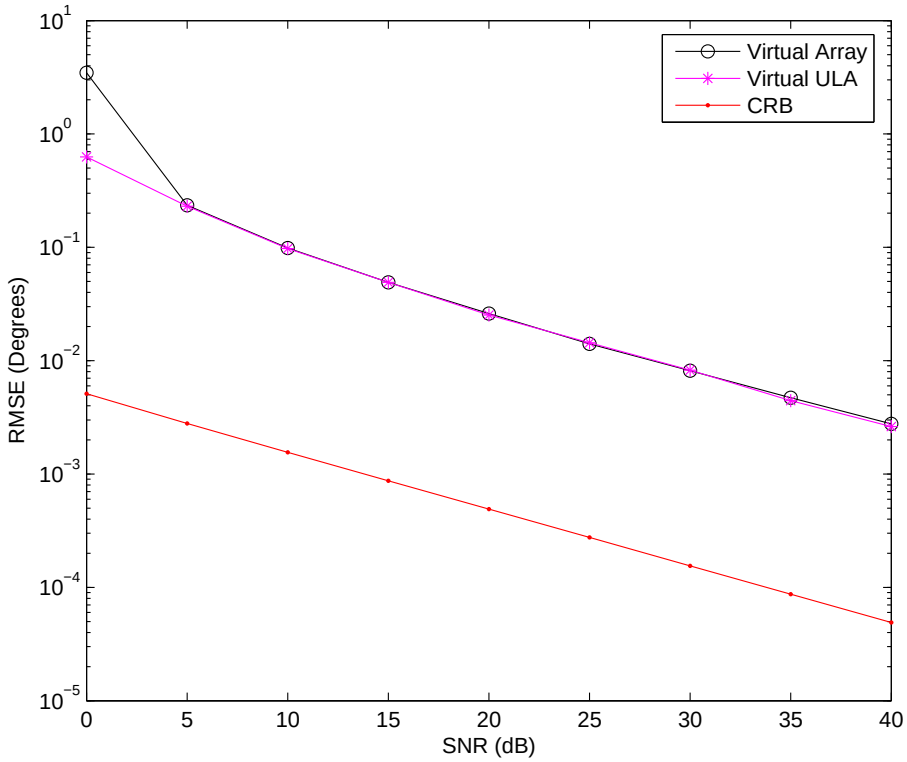

Figure 5.23: Performances of two interpolation methods compared with CRB for three equipower sources with DOA angles 58^o, 63^o and 70^o one of which is coherent with correlation coefficient $\alpha = 0.7391$ and $\beta = 0.3061$.(Interpolation sector $[45^o\ 72^o]$).

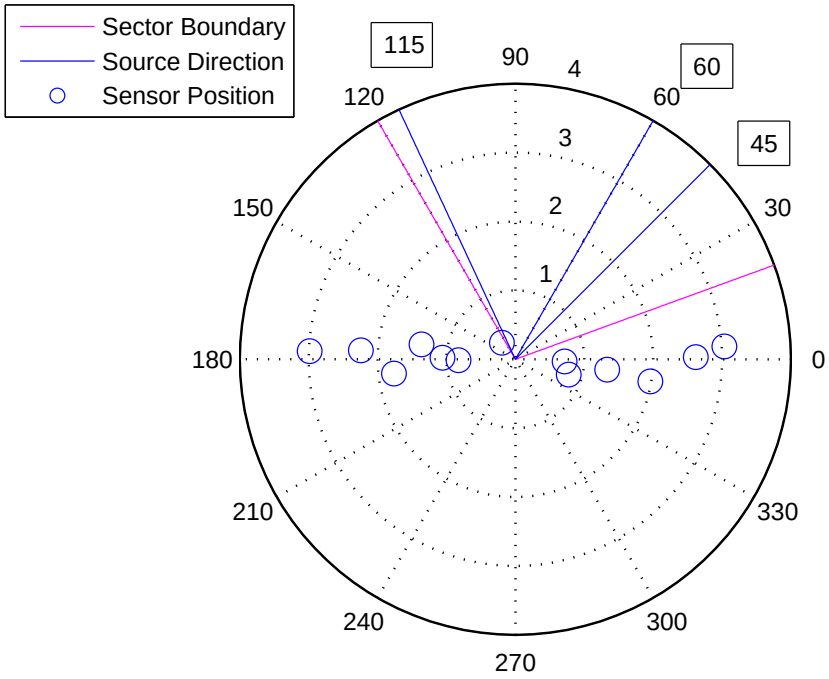

Figure 5.24: The interpolation sector and the sources impinging on the real array

5.24. The DOA estimation RMSE versus SNR is plotted and compared with the stochastic CRB for the two interpolation methods.

In Figure 5.25 DOA estimation RMSE for the two interpolation methods versus SNR compared with stochastic CRB is shown. For this case since the interpolation sector is taken broad for low SNR values the RMSE is very high compared to the stochastic CRB.

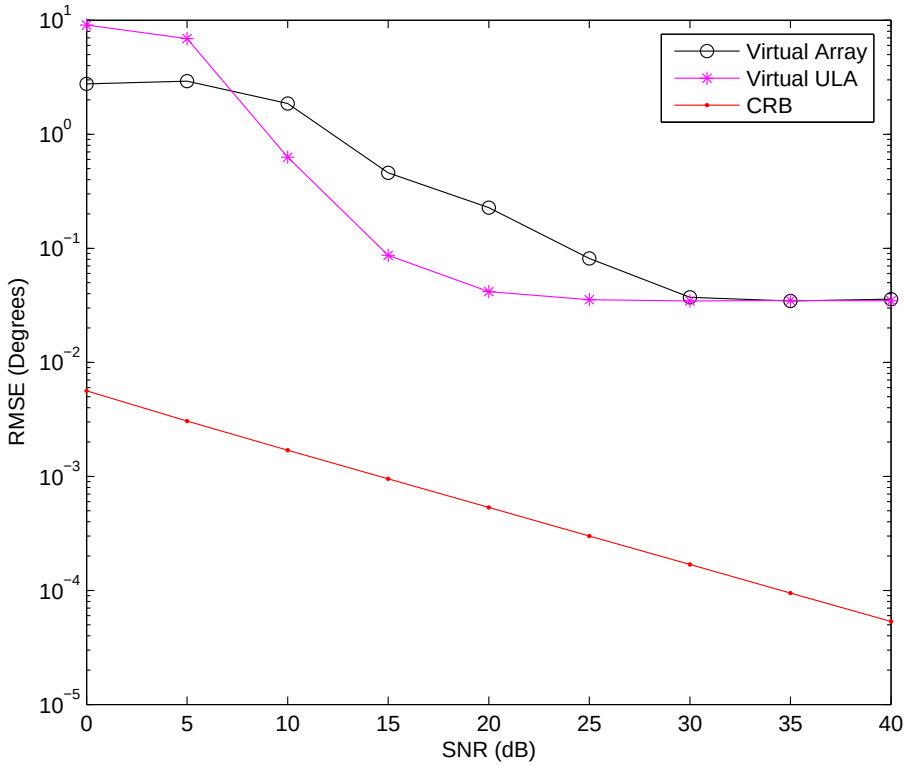

Figure 5.25: Performances of two interpolation methods compared with CRB for three equipower sources with DOA angles 45^o, 60^o and 115^o two of which are coherent with correlation coefficient $\alpha = 0.4, -0.3$ and $\beta = 0.8, -0.7$ respectively .(Interpolation sector $[20^o\ 120^o]$).

5.2.3 Four Sources

Four equipower sources are created at fixed DOA angles 15^o 45^o, 60^o and 115^o and three of them are correlated with correlation coefficient $\alpha = 0.4, -0.3, 0.5$ and $\beta = 0.8, -0.7, -0.6$. SNR level is changed from 0 dB to 40 dB. The interpolation sector for this simulation is chosen as $[0^o\ 120^o]$. The interpolation sector and the sources impinging on the array elements are seen in Figure 5.26. The DOA estimation RMSE versus SNR is plotted and compared with the stochastic CRB for the two interpolation methods. In Figure 5.27 DOA estimation RMSE for the two interpolation methods versus SNR compared with stochastic CRB is shown. For this case since the interpolation sector is taken broad for low SNR values the RMSE is very high compared to the stochastic CRB.

5.3 Virtual Array With Less Array Elements

The mathematical complexity of the DOA estimation algorithm increases as the number of array elements are increased. In order to reduce the mathematical complecity, the number of the virtual array elements can be decreased. However, this is acceptable, only if the interpolation quality isn't affected by the reduction of the number of elements. In order to explore the effect of element reduction, 13 element real array is interpolated toa 8 array element and the interpolation quality is explored. The measure of interpolation quality is the frobenius norm ratio. The sector width versus Frobenius norm ratio is plotted for 13 element interpolated array and 8 element interpolated array on the same Figure which are obtained by the two different interpolation method. The plot is seen in Figure 5.28. The interpolation quality isn't reduced by element number reduction.

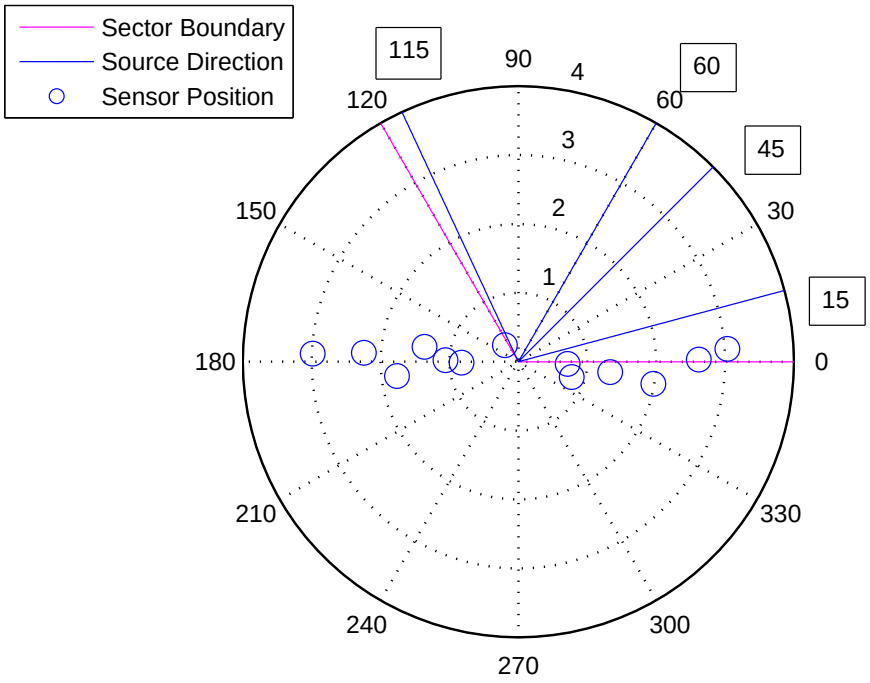

Figure 5.26: The interpolation sector and the sources impinging on the real array

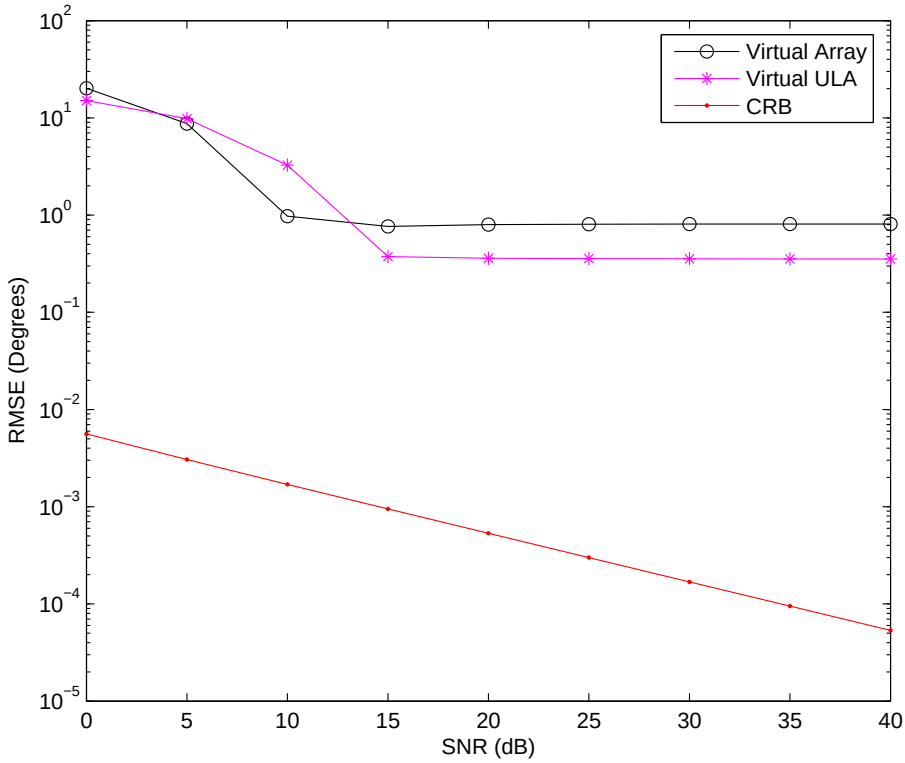

Figure 5.27: Performances of two interpolation methods compared with CRB for four equipower sources with DOA angles 15^o,45^o, 60^o and 115^o three of which are coherent with correlation coefficient $\alpha = 0.4, -0.3, 0.5$ and $\beta = 0.8, -0.7, -0.6$ respectively .(Interpolation sector $[0^o\ 120^o]$).

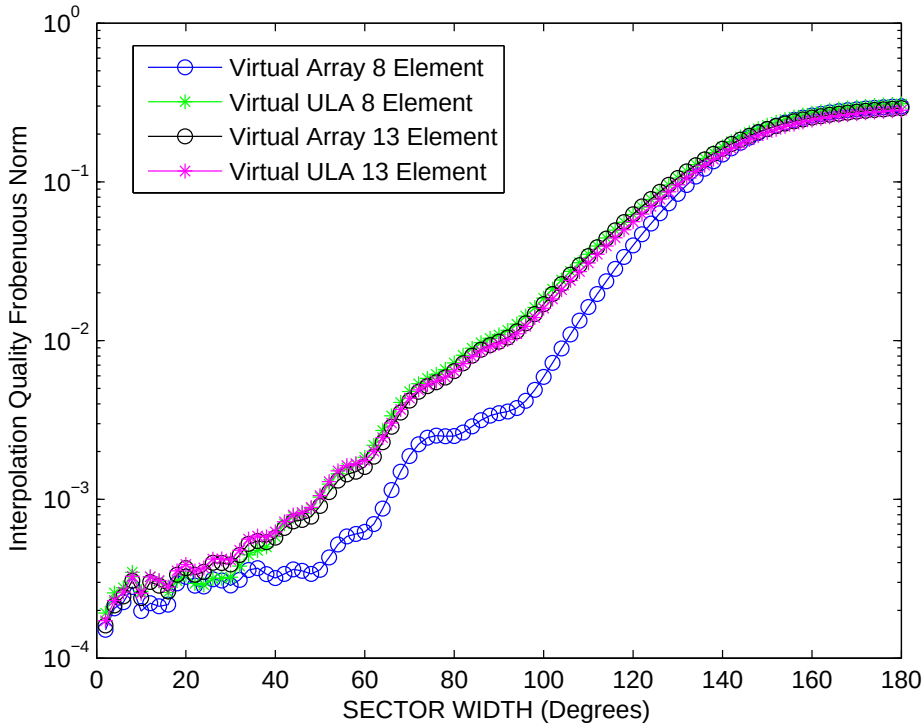

Figure 5.28: Interpolation quality comparison for 8 element interpolated array and 13 element interpolated array

CHAPTER 6

CONCLUSION

In this thesis, DOA estimation with interpolated array using root-MUSIC algorithm for arbitrary array geometries has been examined. Two different methods for designing interpolated array have been implemented. The two methods differ in the selection of the virtual array. For arbitrary array geometry, two interpolation matrices are obtained within a sector using the mentioned methods. The accuracies of the interpolators are investigated in terms of the ratio of the frobenius norm of the interpolation error to the frobenius norm of the array manifold matrix within the sector. It is observed that both the two methods give almost the same interpolation quality and the interpolation quality increases as the sector width decreases, however the condition number of the interpolation matrix gets larger. The sector width partition is another important thing that affects the interpolation error. As the sector width partition gets larger the interpolation quality increases, however after at some value it is seen that it doesn't result in any increase in the interpolation quality. The simulation experiment for the interpolated root-MUSIC using the two interpolation methods has seemed to result in very similar results. They both give close values to the MUSIC algorithm applied to real array geometry if the interpolator is designed properly. In the virtual ULA method the design of the virtual array is under the control of the designer. The placement of virtual array elements is done by the designer and generally the virtual elements are placed as close as possible to the real elements. Another approach is to place array elements to the

perpendicular axis to the interested sector. However, the placement of this type doesn't result in an increase in the interpolator quality for arbitrary array geometries which are almost linear. In the second interpolation method, the designer can't choose the virtual array elements, because the result of virtual array method is not a physical array. It is a virtual array manifold vector having the same differential behavior as the real array manifold vector within the selected sector. Spatial smoothing algorithm is implemented and the performance evaluation is done by using the two interpolation methods. Spatial smoothing preprocessing performance was evaluated in an early work by Friedlander [11] using virtual ULA. However, in this work spatial smoothing is applied to a non-real virtual array having the necessary Vandermonde structure and the same performance as in the virtual ULA case is obtained in the simulations.

REFERENCES

[1] A.J.Barabell"Improving the resolution performance of eigenstructure based direction finding algorithms. " *Proc. ICASSP ,* pages 336-339, Boston, MA, 1983

[2] M.S.Barlett, "Smoothing periodograms from time series with continuous spectra " *Nature*, 161:686-687,1948.

[3] G.Bienvenu and L.Kopp"Adaptivity to background noise spatial coherence for high resolution passive methods. " *Proc. ICASSP,* vol.1, pp.307-310, Denver, Colorado, April 1980.

[4] G.Bienvenu and L.Kopp"Optimality of high resolution array processing using the eigensystem approach. " *IEEE Trans. Acoustic, Speech, Signal Processing,* vol.ASSP-31, pp. 1234-1248, October 1983

[5] J.F.Böhme,"Estimation of spectral Parameters of correlated signals in wavefields " *Signal Processing* . vol.11, pp.329-337, 1986.

[6] M.Bühren, M.Pesavento and J.F.Bö hme"Virtual array design for array interpolation using differential geometry" *Proc.*ICASSP'04

[7] J.Capon, "High resolution Frequency-Wavenumber Spectrum Analysis " *Proc. IEEE*, 57(8):2408-1418,Aug. 1969.

[8] J.E.Evans, J.R.Johnson, and D.F.Sun "Application of advanced signal processing techniques to angle of arrival estimation in ATC navigation and surveillance system " M.I.T Lincoln Lab, Lexington, MA, Rep. 582, 1982.

[9] B.Friedlander and A.J.Weiss, "Direction finding Using interpolated arrays " Report SPT-89-001-NE, Signal Processing Technology, February 1990.

[10] B.Friedlander, "Direction finding with an interpolated array " in *Proc. ICASSP 90*, Albuquerque, NM, pp.2951-2954 December 1990.

[11] Friedlander, B., Weiss, A.J., "Direction finding using spatial smoothing with interpolated arrays " *IEEE Trans. on Aerospace and Electronic Systems*

[12] B.Friedlander"The root-MUSIC algorithm for direction finding with interpolated arrays " *Signal Processing.* vol.30, pp.15-29,1993 .

[13] A.B.Gershman and J.F.Böhme "A note on most favorable array geometries for DOA estimation and array interpolation . " *IEEE Signal Processing Letters,* vol.4 No.8, August 1997

[14] Gershman, A.B., Stoica, P., Pesavento, M. and Larsson, E.G., "Stochastic Cramer-Rao bound for direction estimation in unknown noise fields," *Radar, Sonar and Navigation, IEE Proceedings*, vol.149, no.1, pp.2–8, February 2002.

[15] P.Hyberg, M.Jansson and B.Ottersten"Array mapping:optimal transformation matrix design" *Proc.*ICASSP'02, Orlando, Florida, pp.2905-2908, May 2002 .

[16] T.J.Shan, T.Kailath and M.Wax "On spatial smoothing direction of arrival estimation of coherent signals. " *IEEE Trans. on ASSP. ,* ASSP33(4) pages 806-811, August 1985

[17] A.Manikas,N.H.Dowlut"The use of differential geometry in array signal processing " *Kybernetes* vol.27, no.3, pp.251-163,1998 .

[18] Hyberg, P., Jansson, M., Ottersten, B., "Array Interpolation and DOA MSE Reduction " *IEEE Trans. on Signal Processing*, pp.4464 - 4471, Vol. 53, No.12, Dec. 2005.

[19] A.Paulraj and T.Kailath"A subspace rotation approach to signal parameter estimation. " *Proc. IEEE ,* pages 1044-1045, July 1986

[20] S.U.Pillai, and B.H.Kwon"Forward/backward spatial smoothing techniques for coherent signal identification " *IEEE Trans. Acoust., Speech, Signal Processing*, vol.37 ,no.1,pp.8-15, Jan. 1989.

[21] B.D.Rao and K.V.S.Hari, "Performance Analysis of Root-MUSIC " *IEEE Trans. Acoustics Speech and Signal Processing*, December 1989.

[22] R.Roy and T.Kailath "ESPRIT-Estimation of signal parameters via rotational invariance techniques. " *IEEE Trans. on ASSP. ,* ASSP37(7) pages 984-995, July 1989

[23] Scharf, L.L. and McWhorter, L.T., "Geometry of the Cramer-Rao bound,"*Statistical Signal and Array Processing, 1992. Conference Proceedings., IEEE Sixth SP Workshop on*, pp.5–8, 7–9 October 1992

[24] R.O.Schmidt"Multiple emitter location and signal parameter estimation. " *Proc. RADC Spectrum Estimation Workshop,* Griffiths AFB, Rome, New York, pp.243-258, 1979

[25] R.O.Schmidt *Multiple emitter location and signal parameter estimation.* PhD Dissetatation, Stanford University, Stanford, California, 1981

[26] R.O.Schmidt"New mathematical tools in direction finding and spectral analysis. " *Proc. SPIE 27th Ann. Symp.,* San Diego, California, August 1983.

[27] T.J.Shan, M.Wax, and T.Kailath "On spatial smoothing of estimation of coherent signals " *IEEE Trans. Acoust., Speech, Signal Processing*, vol. ASSP-33,pp.806-811, Aug. 1985.

[28] Stoica, P. and Nehorai Arye, "MUSIC, maximum likelihood, and Cramer-Rao bound," *Acoustics, Speech, and Signal Processing [see also IEEE Transactions on Signal Processing], IEEE Transactions on*, vol.37, no.5, pp.720–741, May 1989.

[29] Stoica, P., Nehorai, A., "MUSIC, maximum likelihood, and Cramer-Rao bound: further results and comparisons," *Acoustics, Speech, and Signal Processing [see also IEEE Transactions on Signal Processing], IEEE Transactions on*, vol.38, no.12, pp.2140–2150, December 1990.

[30] Stoica, P., Jian Li, "Study of the Cramer-Rao bound as the numbers of observations and unknown parameters increase," *Signal Processing Letters, IEEE* vol.3, no.11, pp.299–300, November 1996.

[31] Stoica, P., Larsson, E.G., Gershman, A.B. "The stochastic CRB for array processing: a textbook derivation " *IEEE Signal Processing Letters*, pp.148-150, Vol. 8, Issue 5, May 2001

[32] Stoica, P. and Moses R., "Spectral Analysis of Signals."Prentice-Hall, Upper Saddle River, NJ, 2005.

[33] T.K. Yaşar, "Improvements in DOA Estimation By Array Interpolation in Non-Uniform Linear Arrays."Thesis Work, METU, August 2006.

[34] Weiss, A.J. and Friedlander, B., "On the Cramer-Rao Bound for Direction Finding of Correlated Signals,"*Signal Processing, IEEE Transactions on [see also Acoustics, Speech, and Signal Processing, IEEE Transactions on]* vol.41, no.1, pp.495–, Jan 1993.